 doi:10.20944/preprints202109.0048.v1

Research article

UHPLC-Orbitrap-HRMS Identification of 51 Oleraceins (Cyclo-Dopa Amides) in *Portulaca oleracea* L. Cluster Analysis and MS² Filtering by Mass Difference

Yulian Voynikov[1,*], Paraskev Nedialkov[2], Reneta Gevrenova[2], Dimitrina Zheleva-Dimitrova[2], Vessela Balabanova[2], Ivan Dimitrov[1]

[1] Medical University, Faculty of Pharmacy, Department of Chemistry, 2 Dunav str., 1000 Sofia, Bulgaria
[2] Medical University, Faculty of Pharmacy, Department of Pharmacognosy, 2 Dunav str., 1000 Sofia, Bulgaria
* Correspondence: y_voynikov@pharmfac.mu-sofia.bg

Abstract: Oleraceins are a class of indoline amide glycosides found in *Portulaca oleracea* L. (Portulacaceae), or purslane. These compounds are characterized with 5,6-dihydroxyindoline-2-carboxylic acid *N*-acylated with cinnamic acid derivatives, and many are glucosylated. Herein, hydromethanolic extracts of the aerial parts of purslane were subjected to UHPLC-Orbitrap-HRMS analysis, conducted in negative ionization mode. Diagnostic ion filtering (DIF), followed by diagnostic difference filtering (DDF), were utilized to automatically filter out MS data and select plausible oleracein structures. After an in-depth MS² analysis, a total of 51 oleracein compounds were tentatively identified. Of them, 26 had structure matching one of already known oleraceins and the other 25 are new, undescribed in the literature structures, belonging to the oleracein class. Moreover, diagnostic fragment ions were selected, based on which clustering algorithms and visualizations were employed. As we demonstrate, clustering methods can provide valuable insights into the mass fragmentation elucidation of natural compounds in complex mixtures.

Keywords: orbitrap; purslane; oleracein; diagnostic ion; diagnostic difference; clustering methods

1. Introduction

Portulaca oleracea L. (Portulacaceae), or purslane, is a widely spread annual plant found in many parts of the world. Purslane is considered an edible vegetable in many areas of Europe, the Mediterranean, and tropical Asian countries, and added in soups and salads [1-3]. Purslane has been used in folk and traditional medicine as a remedy for many ailments [4].

There are a number of reports on the ethnomedicinal and pharmacological profiles of purslane [5-7]. Purslane extracts are reported to exhibit various pharmacological activities such as antioxidant [2, 8, 9], anti-inflammatory [10-12], neuroprotective [13-15], antimicrobial [16, 17], antidiabetic [18-20], antiulcerogenic [21], and anticancer [19, 22, 23].

Purslane contain diverse bio-active compounds such as flavonoids, polysaccharides, fatty acids, vitamins and minerals, and alkaloids [1, 2, 4, 5, 24, 25]. Among alkaloids, a class of indoline amide glycosides, called oleraceins or cyclo-dopa amides, have been isolated and characterized in purslane extracts [12, 25-29]. These compounds are characterized with 5,6-dihydroxyindoline-2-carboxylic acid *N*-acylated with cinnamic acid derivatives, and many are highly glucosylated. All sugar moieties in characterized oleraceins in the literature are β-D-glucopyranoses [12, 27, 29]. The majority of the identified oleraceins in the literature are listed in Table 1.

Preprints (www.preprints.org) | NOT PEER-REVIEWED | Posted: 2 September 2021 doi:10.20944/preprints202109.0048.v1

Table 1. Known isolated and characterized oleraceins in the literature: A-D [29]; oleraceins E, T, U, V, W are not included; F and G [30]; H, I, K, L, N-S [27]; X-ZB [12].

Name	R_1	R_2	R_3
Oleracein A	H	H	H
Oleracein B	H	OCH_3	H
Oleracein C	glu	H	H
Oleracein D	glu	OCH_3	H
Oleracein F	H	OCH_3	OCH_3
Oleracein G	H	H	OCH_3

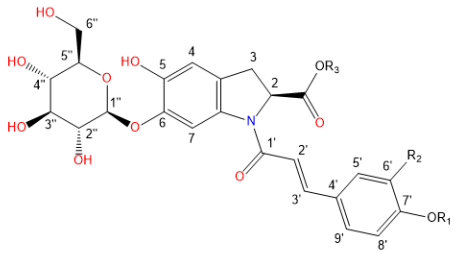

Name	R_1	R_2	R_3	R_4
Oleracein H	H	H	H	H
Oleracein I	H	OCH_3	fer	H
Oleracein K	H	H	H	caff
Oleracein L	H	OCH_3	caff	H
Oleracein N	H	H	fer	H
Oleracein O	glu	H	H	H
Oleracein P	glu	H	H	H
Oleracein Q	H	OCH_3	fer	H
Oleracein R	glu	H	fer	H
Oleracein S	H	H	H	fer
Oleracein X	H	OCH_3	sin	H

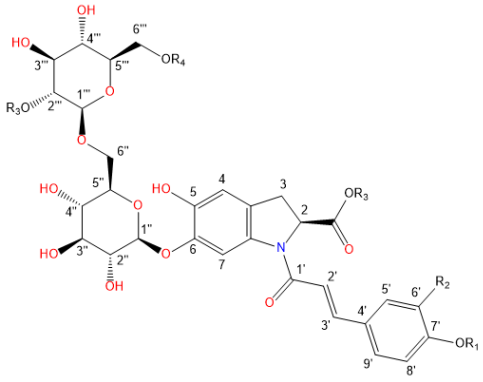

Name	R_1	R_2	R_3	R_4
Oleracein Y	H	H	caff	caff
Oleracein Z	H	H	caff	fer
Oleracein ZA	H	OCH_3	fer	H
Oleracein ZB	H	OCH_3	fer	sin

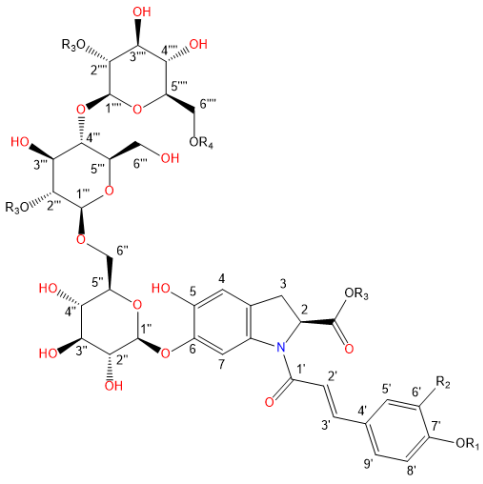

Xiang et al. [29] were the first to isolate and structurally characterize several of these indoline amides, naming them oleraceins A, B, C, D, and E. Xing et al. [25] identified oleraceins A-D, F, and G by Orbitrap-MS^2 analysis in purslane extracts. Later, Liu et al. [30] isolated oleraceins F and G. Eight more oleraceins H–O were identified by Jiao et al. [26] based on UV and MS^2 fragmentation analysis. A year later, the same team [27] isolated oleraceins H, I, K, L, N–S. Just recently, Fu et al. [12] isolated five new high molecular

Preprints (www.preprints.org) | NOT PEER-REVIEWED | Posted: 2 September 2021 doi:10.20944/preprints202109.0048.v1

weight (> 900 Da) oleraceins, naming them oleracein X, Y, Z, ZA and ZB. In our previous study, 11 oleraceins (A-D, N-Q, S, U and W-glu) were tentatively identified by UHPLC-Orbitrap-MS in positive ionization mode in hydromethanolic extracts of the aerial parts of purslane [28].

Herein, utilizing UHPLC-Orbitrap-HRMS in negative ionization mode, we carried out an extensive identification and characterization of oleraceins in hydromethanolic extracts from the aerial parts of purslane. We limited the MS^2 characterization to oleraceins having mass up to 1 kDa, although heavier ones were also detected. After an in-depth MS^2 analysis, a total of 51 oleracein compounds were tentatively identified and characterized, of which 26 had structure matching one of the already known oleraceins and the other 25 are new, undescribed in the literature structures, belonging to the oleraceins class. Diagnostic ion filtering (DIF) and diagnostic difference filtering (DDF) were utilized to refine the selection of compounds that possess oleracein structure. Additionally, clustering of every oleracein based on their MS^2 features was performed and presented with heatmaps, *k*-means and pam clustering, principal component analysis (PCA) and hierarchical clustering. As we demonstrate, clustering methods can provide valuable insights into the structure elucidation of natural compounds by mass spectrometry in complex mixtures.

2. Results and Discussion

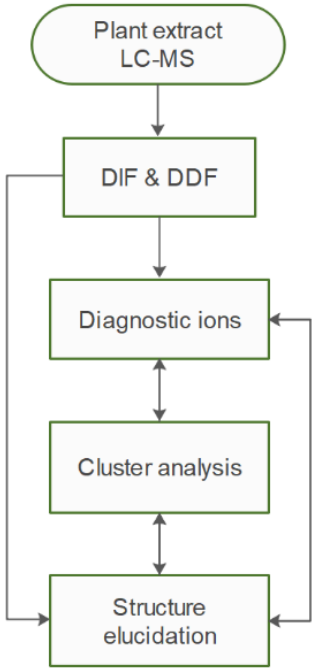

Figure 1. Workflow diagram.

A workflow diagram of the study is shown in Figure 1. In summary, hydromethanolic extract of purslane were obtained, and subjected to HR-MS^2 analysis. The raw data was filtered by DIF and then DDF to select compounds possessing specific fragment ions and specific mass differences for the 5,6-dihydroxyindoline-2-carboxylic acid scaffold, which is common for all oleraceins. The filtered MS^2 data were then analyzed manually to structurally elucidate oleracein compounds. In the course of elucidation, 43 fragment ions were selected as diagnostic fragment ions that were afterwards used to describe every oleracein as a vector with length 43 and values equal to the relative percentage intensities of the diagnostic ions. This permitted to carry out clustering analyses to establish structural similarities between oleracein compounds based on their MS^2 features. The results from the clustering analysis were used to corroborate and supplement the structural elucidation or to correct it.

Oleraceins are characterized with 5,6-dihydroxyindoline-2-carboxylic acid *N*-acylated with either coumaric, caffeic or ferulic acid. Most of them are 6-O glucosylated (Table 1). The sugar moieties of all characterized oleraceins in the literature are identified as β-D-glucopyranoses [12, 27, 29], and so, in this paper, the hexose moieties are regarded as β-D-glucopyranoses.

In our study, the lowest *m/z* oleracein observed was oleracein A with a molecular ion of 502.135 $[M-H]^-$ *m/z*. Other reported in the literature oleraceins with lower mass [29, 30] were not observed in our samples. Our study limited the characterization of oleraceins with mass up to 1kDa, although heavier oleraceins were also detected.

In total of 82 candidate substances were automatically selected, based on the above-mentioned criteria using DIF, followed by DDF, and their MS^2 fragmentation manually inspected. The DDF results are presented in the supplementary material (Table S1) as *m/z* transitions for all identified oleraceins. Of the total 82 candidates, 19 had too low MS^2 intensity (below 1.5E04) and were not interpreted, 12 were false positives (not having oleracein structure), and 51 were identified as oleraceins (Table 2). Of them, 25 are new, undescribed in the literature oleraceins. The other 26 oleraceins were matching a structure

Preprints (www.preprints.org) | NOT PEER-REVIEWED | Posted: 2 September 2021 doi:10.20944/preprints202109.0048.v1

of one of the already known oleraceins: A, B, C, D (2 isoforms), H, I (2 isoforms), J, K, L, M (2 isoforms), N/S (4 isoforms), O (3 isoforms), P, Q, W glu, X (3 isoforms). Table 2 presents the chemical structures of the identified 51 oleraceins and Table 3 provides their chromatographic and mass spectral characteristics. For complete chromatographic and mass spectral data see Table S2 and Table S3.

Table 2. Structure representation of the identified 51 oleraceins. For list of used abbreviations see "4.9. Used abbreviations".

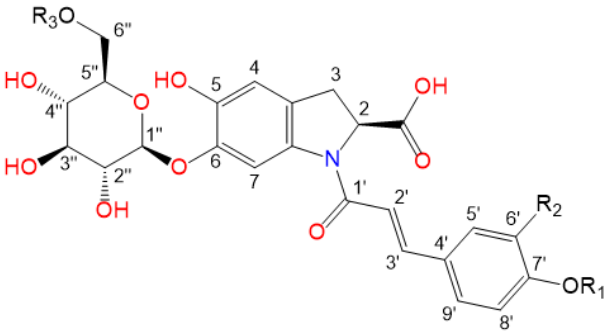

	Compound	Abbrev	R_1	R_2	R_3	Structure match
1	glu-ind-coum	GIC	H	H	H	Oleracein A [29]
2	glu-ind-caff	GIA	H	OH	H	Oleracein W glu [28]
3	glu-ind-fer	GIF	H	OCH_3	H	Oleracein B [29]
4	glu-glu-ind-coum	GGIC	H	H	glu	Oleracein H [27]
5	glu-ind-coum-glu	GICG	glu	H	H	Oleracein C [29]
6	fer-glu-ind-coum	FGIC	H	H	fer	new
7	glu-ind-caff-glu	GIAG	glu	OH	H	new
8	glu-glu-ind-caff	GGIA	H	OH	glu	new
9	glu-ind-fer-glu	GIFG	glu	OCH_3	H	Oleracein D [29]
10	glu-ind-fer-glu	GIFG.1	glu	OCH_3	H	Oleracein D [29]
11	glu-glu-ind-fer	GGIF	H	OCH_3	glu	Oleracein I [27]
12	glu-glu-ind-fer	GGIF.1	H	OCH_3	glu	Oleracein I [27]
13	sin-glu-ind-coum	SGIC	H	H	sin	new
14	fer-glu-ind-fer	FGIF	H	OCH_3	fer	new
15	sin-glu-ind-caff	SGIA	H	OH	sin	new
16	sin-glu-ind-fer	SGIF	H	OCH_3	sin	new
17	hb-glu-glu-ind-coum	OGGIC	H	H	hb-glu	new
18	coum-glu-glu-ind-coum	CGGIC	H	H	coum-glu	new
19	caff-glu-glu-ind-coum	AGGIC	H	H	caff-glu	Oleracein K [27]
20	glu-glu-ind-coum-glu	GGICG	glu	H	glu	Oleracein P [27]
21	fer-glu-ind-coum-glu	FGICG	glu	H	fer	new
22	fer-glu-glu-ind-coum	FGGIC	H	H	fer-glu	Oleracein N/S [27]
23	fer-glu-glu-ind-coum	FGGIC.1	H	H	fer-glu	Oleracein N/S [27]
24	fer-glu-glu-ind-coum	FGGIC.2	H	H	fer-glu	Oleracein N/S [27]
25	fer-glu-glu-ind-coum	FGGIC.3	H	H	fer-glu	Oleracein N/S [27]
26	caff-glu-glu-ind-caff	AGGIA	H	OH	caff-glu	new
27	glu-glu-ind-caff-glu	GGIAG	glu	OH	glu	new
28	caff-glu-glu-ind-fer	AGGIF	H	OCH_3	caff-glu	Oleracein L [27]

Preprints (www.preprints.org) | NOT PEER-REVIEWED | Posted: 2 September 2021 doi:10.20944/preprints202109.0048.v1

29	fer-glu-glu-ind-caff	FGGIA	H	OH	fer-glu	Oleracein J [26]
30	glu-glu-ind-fer-glu	GGIFG	glu	OCH_3	glu	Oleracein Q [27]
31	fer-glu-glu-ind-fer	FGGIF	H	OCH_3	fer-glu	Oleracein O [27]
32	fer-glu-glu-ind-fer	FGGIF.1	H	OCH_3	fer-glu	Oleracein O [27]
33	fer-glu-glu-ind-fer	FGGIF.2	H	OCH_3	fer-glu	Oleracein O [27]
34	sin-glu-glu-ind-coum	SGGIC	H	H	sin-glu	Oleracein M [26]
35	sin-glu-glu-ind-coum	SGGIC.1	H	H	sin-glu	Oleracein M [26]
36	glu-fer-ind-fer-glu	GFGIF	H	OCH_3	glu-fer	new
37	glu-fer-ind-fer-glu	GFGIF.1	H	OCH_3	glu-fer	new
39	sin-glu-ind-coum-glu	SGICG	glu	H	sin	new
40	sin-glu-glu-ind-caff	SGGIA	H	OH	sin-glu	new
38	sin-glu-glu-ind-fer	SGGIF	H	OCH_3	sin-glu	Oleracein X [12]
41	sin-glu-glu-ind-fer	SGGIF.1	H	OCH_3	sin-glu	Oleracein X [12]
42	sin-glu-glu-ind-fer	SGGIF.2	H	OCH_3	sin-glu	Oleracein X [12]
43	glu-sin-glu-ind-fer	GSGIF	H	OCH_3	glu-sin	new
44	hb-glu-glu-ind-coum-glu	OGGICG	glu	H	hb-glu	new
45	glu-caff-glu-glu-ind-coum	GAGGIC	H	H	glu-caff-glu	new
46	glu-caff-glu-glu-ind-coum	GAGGIC.1	H	H	glu-caff-glu	new
47	caff-glu-glu-glu-ind-coum	AGGGIC	H	H	caff-glu-glu	new
48	caff-glu-glu-ind-coum-glu	AGGICG	glu	H	caff-glu	new
49	glu-glu-glu-ind-coum-glu	GGGICG	glu	H	glu-glu	new
50	glu-glu-ind-coum-glu-glu	GGGICG.1	glu-glu	H	glu	new
51	glu-glu-glu-ind-coum-glu	GGICGG	glu	H	glu-glu	new

Table 3. Chromatographic and mass spectral features of the identified 51 oleraceins.

	Abbrev	**exact m/z**	**MS^2**	**rt (min)**	**Structure match**
1	GIC	502.1355	502.1354 (3.57), 340.0826 (45.06), 296.0927 (16.56), 268.0978 (2.50), 202.0509 (1.70), 194.0458 (28.87), 150.0560 (5.99), 148.0403 (4.20), 145.0294 (100)	10.54	Oleracein A [29]
2	GIA	518.1304	518.1303 (0.75), 356.0775 (43.12), 246.0407 (49.23), 202.0509 (27.05), 194.0458 (32.49), 161.0243 (100), 150.0560 (8.43), 148.0403 (2.46)	9.07	Oleracein W glu [28]
3	GIF	532.1460	532.1460 (3.76), 370.0931 (60.33), 326.1033 (22.89), 298.1084 (4.41), 194.0458 (42.41), 175.0400 (100), 161.0243 (11.88), 160.0165 (13.6), 150.0560 (8.42), 148.0403 (5.95)	11.23	Oleracein B [29]
4	GGIC	664.1883	664.1882 (5.98), 518.1514 (65.37), 340.0826 (17.09), 296.0927 (35.29), 268.0978 (0.84), 202.0509 (2.79), 194.0458 (100), 150.0560 (34.78), 148.0403 (9.65), 145.0294 (56.75)	8.98	Oleracein H [27]
5	GICG	664.1883	502.1354 (36.75), 340.0826 (85.46), 296.0927 (29.99), 268.0978 (10.68), 202.0509 (2.70), 194.0458 (24.46), 150.0560 (2.80), 148.0403 (5.44), 145.0294 (100)	7.30	Oleracein C [29]
6	FGIC	678.1828	532.1460 (10.94), 502.1354 (0.61), 340.0826 (31.99), 337.0928 (11.78), 296.0927 (11.26), 202.0509 (1.50), 194.0458 (29.34), 193.0506 (3.38), 179.0349 (0.51), 175.0400 (12.68), 161.0243	16.63	new

			(6.46), 160.0165 (2.07), 150.0560 (7.25), 148.0403 (5.18), 145.0294 (100)		
7	GIAG	680.1832	518.1303 (25.28), 356.0775 (89.56), 246.0407 (66.10), 202.0509 (31.77), 194.0458 (19.02), 161.0243 (100), 150.0560 (2.52), 148.0403 (1.91)	7.26	new
8	GGIA	680.1832	680.1831 (1.22), 518.1514 (41.76), 356.0775 (45.60), 246.0407 (52.48), 202.0509 (28.04), 194.0458 (100), 161.0243 (89.61), 150.0560 (29.03), 148.0403 (7.30)	7.81	new
9	GIFG	694.1989	532.1460 (17.77), 370.0931 (100), 326.1033 (23.59), 298.1084 (16.57), 194.0458 (17.63), 175.0400 (78.68), 161.0243 (9.61), 160.0165 (3.28), 150.0560 (3.46), 148.0403 (9.41)	5.91	Oleracein D [29]
10	GIFG.1	694.1989	532.1460 (28.29), 370.0931 (100), 326.1033 (37.46), 298.1084 (19.50), 194.0458 (27.75), 175.0400 (86.22), 161.0243 (17.92), 160.0165 (6.93), 150.0560 (5.42), 148.0403 (7.20)	8.05	Oleracein D [29]
11	GGIF	694.1989	518.1514 (52.21), 370.0931 (24.35), 326.1033 (39.63), 194.0458 (100), 175.0400 (45.92), 161.0243 (18.24), 160.0165 (1.96), 150.0560 (27.72), 148.0403 (12.13)	6.78	Oleracein I [27]
12	GGIF.1	694.1989	694.1988 (9.12), 518.1514 (61.6), 370.0931 (24.57), 326.1033 (48.09), 298.1084 (0.65), 202.0509 (1.54), 194.0458 (100), 175.0400 (43.80), 161.0243 (22.26), 160.0165 (6.29), 150.0560 (31.35), 148.0403 (12.94)	9.64	Oleracein I [27]
13	SGIC	708.1934	562.1565 (6.41), 367.1034 (10.55), 340.0826 (30.31), 296.0927 (10.55), 268.0978 (0.71), 223.0611 (2.45), 205.0505 (9.60), 202.0509 (1.66), 194.0458 (26.35), 191.0349 (5.99), 150.0560 (8.36), 148.0403 (4.64), 145.0294 (100)	16.41	new
14	FGIF	708.1934	532.1460 (7.19), 370.0931 (35.83), 337.0928 (13.32), 326.1033 (14.97), 298.1084 (0.95), 194.0458 (30.33), 193.0506 (1.51), 175.0400 (100), 161.0243 (12.69), 160.0165 (17.46), 150.0560 (9.08), 148.0403 (6.21)	16.89	new
15	SGIA	724.1883	356.0775 (31.93), 246.0407 (42.83), 205.0505 (1.43), 202.0509 (25.69), 194.0458 (21.89), 161.0243 (100), 150.0560 (3.33), 148.0403 (1.96)	15.05	new
16	SGIF	738.2040	562.1565 (6.43), 532.1460 (0.56), 370.0931 (46.26), 367.1034 (14.50), 326.1033 (16.25), 298.1084 (1.23), 223.0611 (3.09), 205.0505 (15.1), 202.0509 (1.67), 194.0458 (38.53), 191.0349 (9.45), 175.0400 (100), 161.0243 (11.90), 160.0165 (20.90), 150.0560 (10.78), 148.0403 (8.52)	16.66	new
17	OGGIC	784.1883	638.1727 (79.93), 518.1514 (17.28), 443.1195 (23.46), 340.0826 (11.79), 194.0458 (98.68), 150.0560 (15.92), 148.0403 (11.58), 145.0294 (38.22), 137.0243 (92.77)	10.61	new
18	CGGIC	810.2251	664.1882 (30.64), 518.1514 (40.17), 518.1514 (19.88), 340.0826 (10.58), 296.0927 (5.81), 194.0458 (100), 150.0560 (24.01), 148.0403 (5.58), 145.0294 (92.62)	11.78	new
19	AGGIC	826.2200	680.1831 (27.17), 664.1882 (15.13), 518.1514 (78.8), 485.1300 (21.36), 356.0775 (1.33), 340.0826 (10.66), 296.0927 (22.75), 194.0458 (100), 179.0349 (8.31), 161.0243 (92.81), 150.0560 (26.74), 148.0403 (11.08), 145.0294 (36.92)	10.59	Oleracein K [27]
20	GGICG	826.2411	664.1882 (18.22), 518.1514 (36.79), 502.1354 (33.23), 340.0826 (59.20), 296.0927 (100), 268.0978 (10.38), 202.0509 (6.37), 194.0458 (37.51), 150.0560 (9.62), 148.0403 (9.67), 145.0294 (84.05)	6.34	Oleracein P [27]
21	FGICG	840.2357	532.1460 (8.85), 502.1354 (15.88), 340.0826 (62.02), 337.0928 (10.42), 296.0927 (26.3), 268.0978 (7.66), 202.0509 (3.70),	13.31	new

			194.0458 (17.58), 193.0506 (2.93), 175.0400 (10.15), 161.0243 (3.16), 160.0165 (2.56), 150.0560 (3.66), 148.0403 (5.79), 145.0294 (100)		
22	FGGIC	840.2357	694.1988 (14.74), 518.1514 (50.03), 502.1354 (2.97), 499.1457 (10.28), 340.0826 (31.03), 296.0927 (23.19), 268.0978 (2.50), 194.0458 (100), 193.0506 (21.57), 175.0400 (39.49), 150.0560 (25.63), 148.0403 (15.82), 145.0294 (96.89)	10.17	Oleracein N/S [27]
23	FGGIC.1	840.2357	694.1988 (23.48), 664.1882 (8.66), 518.1514 (53.69), 499.1457 (15.94), 485.1300 (1.22), 340.0826 (23.33), 296.0927 (23.23), 202.0509 (3.31), 194.0458 (100), 193.0506 (20.73), 175.0400 (32.55), 161.0243 (8.61), 160.0165 (7.44), 150.0560 (34.59), 148.0403 (13.45), 145.0294 (79.11)	11.95	Oleracein N/S [27]
24	FGGIC.2	840.2357	694.1988 (13.14), 664.1882 (4.40), 518.1514 (57.28), 499.1457 (4.07), 340.0826 (25.01), 296.0927 (23.14), 194.0458 (100), 193.0506 (13.25), 175.0400 (13.96), 161.0243 (2.36), 160.0165 (2.86), 150.0560 (27.76), 148.0403 (6.38), 145.0294 (85.71)	14.09	Oleracein N/S [27]
25	FGGIC.3	840.2357	694.1988 (22.64), 664.1882 (7.55), 518.1514 (58.14), 499.1457 (14.77), 485.1300 (1.82), 340.0826 (23.64), 296.0927 (25.22), 202.0509 (2.18), 194.0458 (100), 193.0506 (22.07), 175.0400 (34.66), 161.0243 (6.29), 160.0165 (7.44), 150.0560 (27.31), 148.0403 (15.84), 145.0294 (79.33)	12.36	Oleracein N/S [27]
26	AGGIA	842.2149	680.1831 (27.11), 518.1514 (65.15), 485.1300 (19.31), 356.0775 (23.66), 246.0407 (15.54), 202.0509 (4.30), 194.0458 (84.83), 179.0349 (3.45), 161.0243 (100), 150.0560 (18.25), 148.0403 (2.81)	9.34	new
27	GGIAG	842.2360	680.1831 (10.18), 356.0775 (67.36), 246.0407 (55.5), 202.0509 (32.63), 194.0458 (45.97), 161.0243 (100), 150.0560 (13.27), 148.0403 (6.58)	6.37	new
28	AGGIF	856.2306	694.1988 (16.68), 680.1831 (26.94), 518.1514 (70.4), 485.1300 (17.91), 370.0931 (11.80), 356.0775 (4.04), 326.1033 (25.35), 246.0407 (6.75), 202.0509 (3.29), 194.0458 (92.93), 179.0349 (8.50), 175.0400 (22.16), 161.0243 (100), 160.0165 (5.79), 150.0560 (32.09), 148.0403 (9.30)	11.09	Oleracein L [27]
29	FGGIA	856.2306	694.1988 (12.95), 518.1514 (23.06), 499.1457 (4.64), 356.0775 (40.26), 246.0407 (47.53), 202.0509 (26.56), 194.0458 (56.81), 193.0506 (7.4), 175.0400 (11.29), 161.0243 (100), 160.0165 (1.18), 150.0560 (17.86), 148.0403 (6.52)	10.69	Oleracein J [26]
30	GGIFG	856.2517	694.1988 (24.29), 532.1460 (16.47), 518.1514 (38.97), 370.0931 (46.21), 326.1033 (100), 298.1084 (9.02), 202.0509 (1.78), 194.0458 (35.00), 175.0400 (44.77), 161.0243 (28.71), 160.0165 (3.10), 150.0560 (6.95), 148.0403 (8.94)	7.04	Oleracein Q [27]
31	FGGIF	870.2462	694.1988 (31.87), 518.1514 (60.12), 499.1457 (5.37), 370.0931 (30.38), 326.1033 (29.67), 194.0458 (97.54), 193.0506 (21.72), 175.0400 (100), 161.0243 (25.47), 160.0165 (22.69), 150.0560 (24.82), 148.0403 (5.17)	10.65	Oleracein O [27]
32	FGGIF.1	870.2462	694.1988 (41.84), 518.1514 (63.14), 499.1457 (15.57), 485.1300 (1.83), 370.0931 (32.46), 326.1033 (31.88), 298.1084 (0.69), 202.0509 (1.89), 194.0458 (100), 193.0506 (27.19), 175.0400 (96.79), 161.0243 (21.81), 160.0165 (20.66), 150.0560 (31.54), 148.0403 (14.20)	12.40	Oleracein O [27]
33	FGGIF.2	870.2462	694.1988 (35.51), 518.1514 (58.24), 499.1457 (16.25), 370.0931 (38.93), 340.0826 (3.32), 326.1033 (30.96), 194.0458 (100),	12.79	Oleracein O [27]

Preprints (www.preprints.org) | NOT PEER-REVIEWED | Posted: 2 September 2021 doi:10.20944/preprints202109.0048.v1

			193.0506 (22.11), 175.0400 (98.98), 161.0243 (21.41), 160.0165 (23.47), 150.0560 (31.12), 148.0403 (15.62), 145.0294 (17.78)		
34	SGGIC	870.2462	724.2093 (23.36), 664.1882 (11.65), 529.1562 (16.21), 518.1514 (64.51), 340.0826 (24.79), 296.0927 (24.15), 268.0978 (0.85), 223.0611 (18.33), 205.0505 (30.61), 202.0509 (3.02), 194.0458 (100), 191.0349 (7.94), 150.0560 (34.8), 148.0403 (14.57), 145.0294 (77.17)	11.71	Oleracein M [26]
35	SGGIC.1	870.2462	724.2093 (9.68), 724.2093 (7.56), 664.1882 (8.12), 518.1514 (60.95), 340.0826 (18.71), 296.0927 (14.97), 205.0505 (8.40), 194.0458 (80.79), 150.0560 (13.70), 148.0403 (14.90), 145.0294 (100)	13.98	Oleracein M [26]
36	GFGIF	870.2462	724.2093 (11.32), 708.1933 (14.05), 694.1988 (9.76), 532.1460 (9.89), 518.1514 (21.93), 502.1354 (1.95), 499.1457 (2.86), 370.0931 (63.44), 337.0928 (2.41), 326.1033 (41.38), 194.0458 (61.09), 193.0506 (6.12), 175.0400 (100), 161.0243 (21.21), 160.0165 (11.32), 150.0560 (13.40), 148.0403 (41.38), 145.0294 (13.40)	14.33	new
37	GFGIF.1	870.2462	708.1933 (15.74), 532.1460 (27.33), 370.0931 (78.17), 337.0928 (13.75), 326.1033 (30.50), 298.1084 (6.09), 202.0509 (0.97), 194.0458 (32.87), 193.0506 (4.70), 175.0400 (100), 161.0243 (22.55), 160.0165 (12.61), 150.0560 (5.25), 148.0403 (8.80)	13.52	new
38	SGICG	870.2462	708.1933 (10.86), 562.1565 (8.41), 502.1354 (20.86), 367.1034 (9.61), 340.0826 (67.95), 296.0927 (25.95), 268.0978 (8.19), 223.0611 (1.97), 205.0505 (6.55), 202.0509 (3.52), 194.0458 (24.53), 191.0349 (3.58), 150.0560 (5.25), 148.0403 (6.75), 145.0294 (100)	13.20	new
39	SGGIA	886.2411	724.2093 (13.2), 518.1514 (23.7), 356.0775 (39.43), 246.0407 (47.59), 223.0611 (5.59), 205.0505 (5.59), 202.0509 (34.3), 194.0458 (61.58), 161.0243 (100), 150.0560 (15.36), 148.0403 (5.91)	10.46	new
40	SGGIF	900.2568	724.2093 (13.98), 518.1514 (57.73), 370.0931 (8.6), 223.0611 (11.15), 205.0505 (12.6), 194.0458 (100), 191.0349 (8.23), 175.0400 (64.27), 150.0560 (14.17), 148.0403 (12.00)	10.56	Oleracein X [12]
41	SGGIF.1	900.2568	694.1988 (13.27), 518.1514 (70.61), 370.0931 (39.16), 326.1033 (21.30), 223.0611 (9.33), 205.0505 (17.65), 194.0458 (94.20), 175.0400 (58.85), 161.0243 (15.23), 150.0560 (42.13)	14.09	Oleracein X [12]
42	SGGIF.2	900.2568	724.2093 (23.6), 694.1988 (15.95), 529.1562 (16.23), 518.1514 (66.44), 370.0931 (31.89), 326.1033 (31.2), 223.0611 (18.25), 205.0505 (30.74), 202.0509 (2.01), 194.0458 (100), 191.0349 (10.59), 175.0400 (64.59), 161.0243 (13.07), 160.0165 (12.38), 150.0560 (29.99), 148.0403 (15.08)	12.12	Oleracein X [12]
43	GSGIF	900.2568	562.1565 (14.07), 532.1460 (17.71), 370.0931 (93.17), 367.1034 (19.66), 326.1033 (29.11), 298.1084 (11.67), 205.0505 (10.66), 202.0509 (2.17), 194.0458 (29.35), 191.0349 (8), 175.0400 (100), 161.0243 (25.28), 160.0165 (14), 150.0560 (2.55), 148.0403 (3.44)	13.41	new
44	OGGICG	946.2623	638.1727 (100), 518.1514 (21.76), 443.1195 (14.11), 340.0826 (9.03), 296.0927 (12.12), 194.0458 (72.48), 150.0560 (21.8), 145.0294 (50.83), 137.0243 (60.3)	8.65	new
45	GAGGIC	988.2728	842.2359 (9.79), 680.1831 (53.3), 664.1882 (14.61), 518.1514 (90.13), 485.1300 (44.78), 340.0826 (7.3), 296.0927 (8.35), 194.0458 (79.91), 179.0349 (21.21), 161.0243 (100), 150.0560 (29.14), 145.0294 (11.9)	9.45	new

Preprints (www.preprints.org) | NOT PEER-REVIEWED | Posted: 2 September 2021 doi:10.20944/preprints202109.0048.v1

46	GAGGIC.1	988.2728	842.2359 (13.29), 826.2199 (12.04), 680.1831 (64.32), 664.1882 (11.38), 518.1514 (85.83), 485.1300 (39.72), 340.0826 (10.79), 296.0927 (26.65), 194.0458 (77.31), 179.0349 (8.74), 161.0243 (100), 150.0560 (21.07), 148.0403 (4.19), 145.0294 (37.59)	8.52	new
47	AGGGIC	988.2728	842.2359 (34.71), 826.2410 (10.08), 680.2043 (100), 340.0826 (2.65), 296.0927 (5.14), 194.0458 (70.43), 161.0243 (62.8), 150.0560 (27.02), 148.0403 (13.54), 145.0294 (18.12)	10.07	new
48	AGGICG	988.2728	826.2410 (20.35), 680.1831 (19.77), 664.1882 (38.74), 518.1514 (49.86), 502.1354 (32.18), 485.1300 (44.02), 340.0826 (42.12), 296.0927 (71.42), 268.0978 (6.94), 202.0509 (4.21), 194.0458 (39.22), 179.0349 (11.46), 161.0243 (100), 150.0560 (9.28), 148.0403 (8.84), 145.0294 (56.04)	7.78	new
49	GGGICG	988.2940	988.2939 (23.62), 826.2410 (32.04), 680.2043 (76.98), 502.1354 (34.71), 340.0826 (63.9), 296.0927 (97.09), 268.0978 (12.36), 202.0509 (6.24), 194.0458 (42.82), 150.0560 (11.81), 148.0403 (16.66), 145.0294 (100)	6.21	new
50	GGGICG.1	988.2940	826.2410 (23.97), 680.2043 (37.17), 502.1354 (29.62), 340.0826 (51.79), 296.0927 (98.85), 194.0458 (35.22), 150.0560 (10.56), 148.0403 (7.48), 145.0294 (100)	6.03	new
51	GGICGG	988.2940	988.2939 (52.98), 664.1882 (98.49), 518.1514 (35.65), 340.0826 (18.49), 296.0927 (100), 194.0458 (26.65), 150.0560 (4.70), 148.0403 (5.22), 145.0294 (75.66)	5.83	new

As mentioned earlier, all identified in the literature oleraceins are *N*-acylated with either coumaric, caffeic or ferulic acid (i.e., bearing the substructure **IC**, **IA**, or **IF**). Each oleracein identified in our study is comprised of either **GIC**, **GIA** or **GIF** alone, or linked with several other moieties that include hydroxybenzoyl (**O**), coumaroyl (**C**), caffeoyl (**A**), feruloyl (**F**), sinapoyl (**S**), and glucopyranosyl (**G**). The presence of either of the below fragments indicates the type of hydroxycinnamic acid (HCA) *N*-linked to the indoline core: *m*/*z* 340.0826 ($C_{18}H_{14}O_6N^-$, [*N*-coumaroyl 5,6-dihydroxyindoline-2-carboxylic acid - H]$^-$), *m*/*z* 356.0765 ($C_{18}H_{14}O_7N^-$, [*N*-caffeoyl 5,6-dihydroxyindoline-2-carboxylic acid - H]$^-$), *m*/*z* 370.0921 ($C_{19}H_{16}O_7N^-$, [*N*-feruloyl 5,6-dihydroxyindoline-2-carboxylic acid - H]$^-$) (Figure 2). In addition, the presence of each of the three HCAs can be confirmed by a set of fragments, including 145.0294 *m*/*z* for coumaroyl (**C**), 161.0244 and 109.0295 *m*/*z* for caffeoyl (**A**), and 175.0401, 161.02442 and 160.0166 *m*/*z* for feruloyl (**F**) moiety. The 5,6-dihydroxyindoline-2-carboxylic acid, or the indoline core, characteristic for every oleracein, is represented with fragment ions 194.0458, 150.0560 and 148.0403 *m*/*z*, in decreasing intensity. Fragment 194.0458 *m*/*z*, as well as the characteristic fragment ions for the HCAs are more prominent in oleraceins with lower mass. Regarding the fragmentation of the glycoside moieties, linked (consecutive) glucopyranoses (as in oleraceins **GGIC** or **GGGICG**) are cleaved in the fragmentation process together, i.e., if consecutive neutral losses of hexoses (-162.053 Da, -$C_6H_{10}O_5$) were observed (like in **GICG**), this suggested the presence of a single **G** substructure. In cases of two or three linked glucopyranoses (like in **GGICGG** or **GGGICG**), then neutral losses of 324.107 Da (-$C_{12}H_{20}O_{10}$) or 486.159 Da (-$C_{18}H_{30}O_{15}$), respectively, were observed.

Preprints (www.preprints.org) | NOT PEER-REVIEWED | Posted: 2 September 2021 doi:10.20944/preprints202109.0048.v1

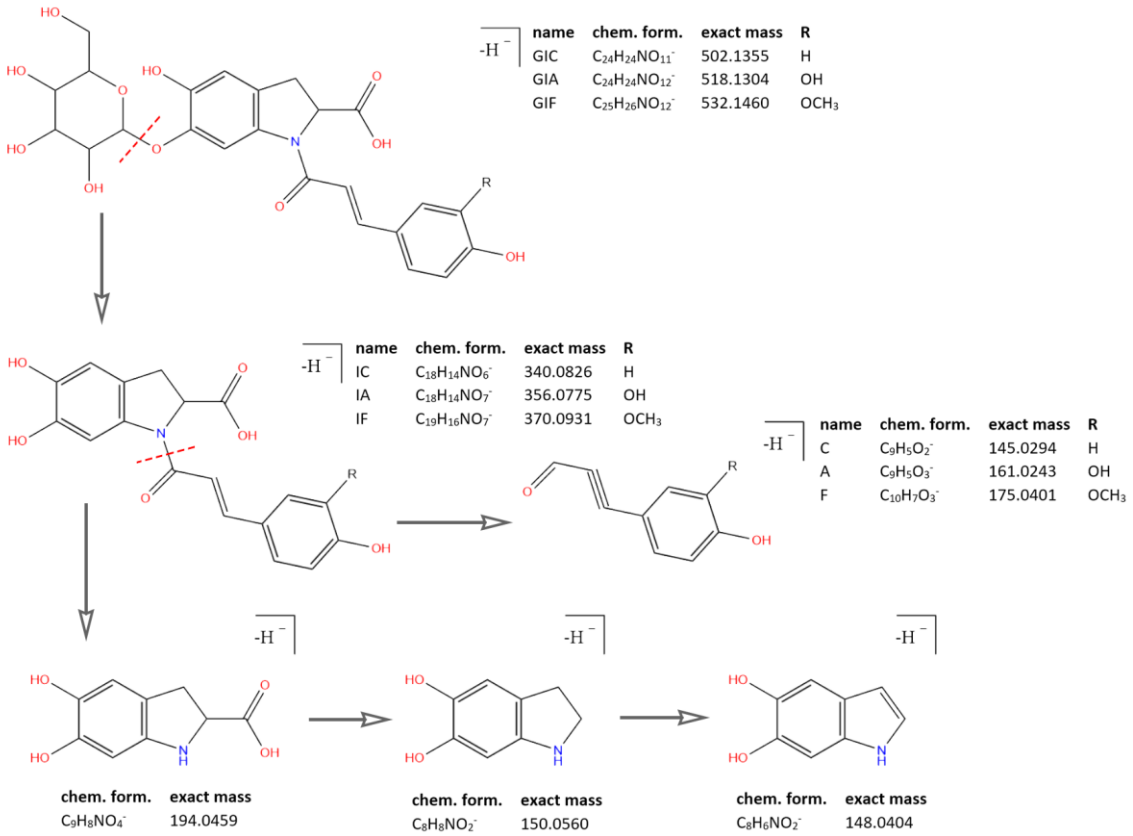

Figure 2. Common fragment ions of the three common substructures in oleraceins: **GIC**, **GIA** and **GIF**.

2.1. Individual MS² fragmentation analysis

Below, the tentative identification of all 51 oleraceins (Table 2 and Table 3) based on high-res MS² fragmentation analysis is described, ordered by increasing mass. Characteristic neutral losses include: CO (-27.995 Da); CO_2 (-43.990 Da); hydroxybenzoyl (**O**) (-120.020 Da); coumaroyl (**C**) (-146.037 Da); caffeoyl (**A**) (-162.032 Da); feruloyl (**F**) (-176.047 Da); sinapoyl (**S**) (-206.054 Da); glucopyranosyl (**G**) (-162.053 Da); double glucopyranosyl (**GG**) (-324.107 Da); triple glucopyranosyl (**GGG**) (-486.159 Da).

The oleracein with the lowest *m/z* identified in our samples bears a precursor ion at 502.135 $[M-H]^-$ *m/z* and elutes at rt 10.54 min. The MS² spectrum displays a fragment ion 340.083 *m/z* (**IC**), formed after a **G** cleavage (-162.053 Da) from the molecular ion. This confirms the *N*-coumaroyl linkage (**IC**). The later undergoes consecutive CO_2 (-43.990 Da) and CO (-27.995 Da) cleavages resulting in 296.093 and 268.098 *m/z*, respectively. The existence of the coumaroyl (**C**) is established by the fragment ions at 145.029, 119.049 and 117.033 *m/z*. The set of fragment ions at 194.046, 150.056 and 148.040 *m/z* confirm the presence of the indoline core (**I**). The proposed structure of this compound is **glu-ind-coum**, or **GIC** and concurs with the structure of oleracein A (Figure 3).

Preprints (www.preprints.org) | NOT PEER-REVIEWED | Posted: 2 September 2021 doi:10.20944/preprints202109.0048.v1

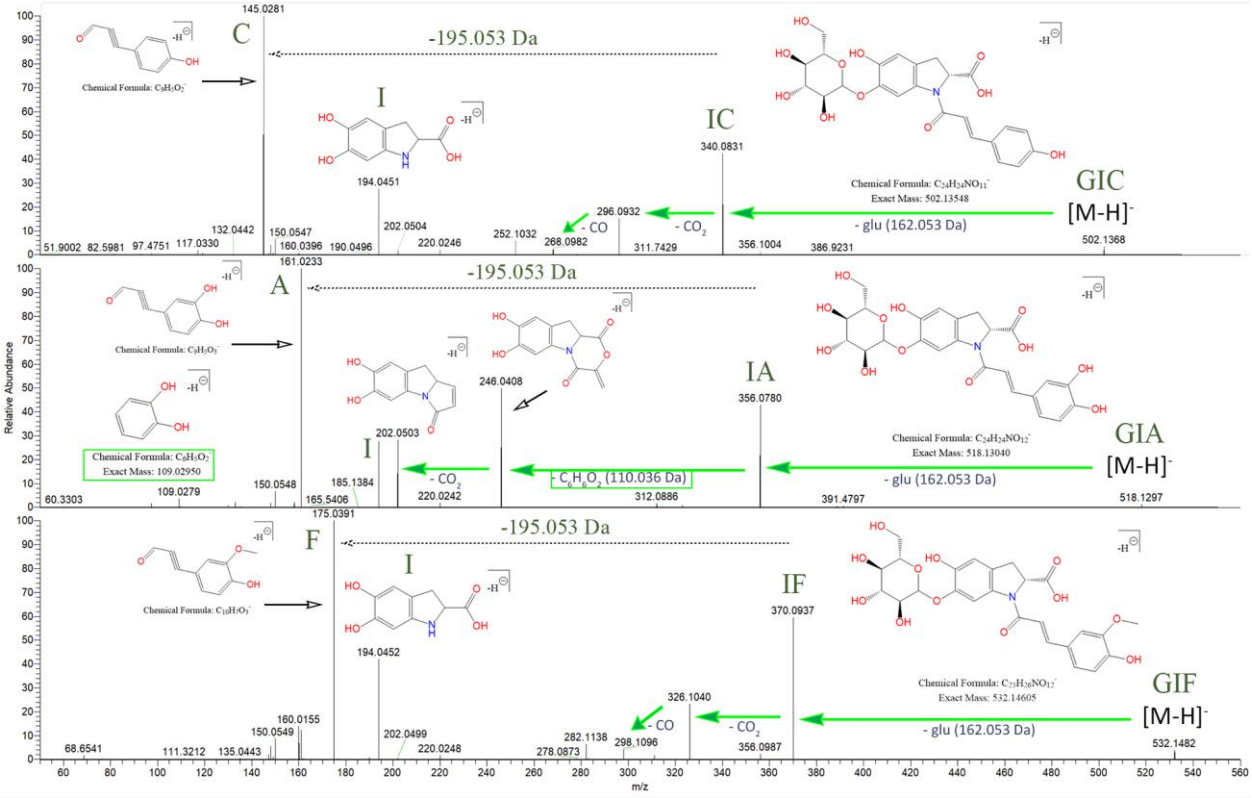

Figure 3. Fragmentation behavior for GIC, GIA, and GIF with proposed chemical structures. The searched specific difference of 195.05316 Da is marked, suggesting a neutral loss of 5,6-dihydroxyindoline-2-carboxylic acid. As shown, IA demonstrates a different fragmentation behavior, compared to IC and IF.

The compound with precursor ion at *m/z* 518.130 [M-H]$^-$, identified as **glu-ind-caff**, or **GIA**, elutes at rt 9.07 min. Fragment ion at 356.078 *m/z* confirms the *N*-caffeoyl linkage (**IA**). Fragment 356.078 *m/z* (**IA**), unlike fragment 340.083 (**IC**), reveals a cleavage of $C_6H_6O_2$ (-110.037 Da) with consequent loss of CO_2, transition 356.078 → 246.041 → 202.051 *m/z* (Figure 3). Fragment 109.028 *m/z* ([$C_6H_6O_2$-H]$^-$) confirms the previous finding. Fragment 356.078 *m/z* is capable of CO_2 cleavage to form fragment 312.088 *m/z*. The **A** and **I** substructures are corroborated by their corresponding fragments. The structure of this compound matches oleracein W glu.

The MS^2 data of the compound with *m/z* 532.146 [M-H]$^-$, eluting at rt 11.23, identified as **glu-ind-fer**, or **GIF**, reveals the set of fragment ions corroborating the **IF** structure, namely 370.093, 326.103, and 298.108 *m/z*, formed in a similar fashion as discussed for **GIC**, after consecutive CO_2 and then CO losses, respectively, from **IF**. The structure of **GIF** coincides with oleracein B (Figure 3).

The base peak chromatogram of *m/z* 664.188 [M-H]$^-$ reveals two peaks eluting at rt 7.32 and 9.00 min. The isobar eluting at 7.32 min was identified as **glu-ind-coum-glu**, or **GICG**. Fragment 340.083 *m/z* confirms the **IC**. The molecular ion can consecutively cleave the two proximal hexoses resulting in the transition 664.188 → 502.135 → 340.083 (**IC**) *m/z*. Then, the fragmentation of 340.083 *m/z* is as described earlier for **GIC**. The proposed structure of **GICG** coincides with oleracein C.

The other isobar eluting at rt 9.00 min is identified as **glu-glu-ind-coum**, or **GGIC**. Fragment ion 340.083 *m/z* confirms the **IC**. The molecular ion can cleave the **C** () resulting in fragment ion 518.151 *m/z* (**GGI**). The subsequent neutral loss of 324.107 Da suggests a joint **GG** loss, resulting in 194.046 *m/z* (**I**). The proposed structure of this compound matches oleracein H.

The compound with *m/z* 678.183 [M-H]$^-$ eluting at rt 16.63 min is identified as **fer-glu-ind-coum**, or **FGIC**. Fragment ion 340.083 *m/z* confirms the **IC**. The molecular ion can cleave either the proximal **C** (-146.037 Da) or **F** (-176.047 Da), resulting in 532.146 *m/z* (**FGI**)

Preprints (www.preprints.org) | NOT PEER-REVIEWED | Posted: 2 September 2021 doi:10.20944/preprints202109.0048.v1

or 502.135 *m/z* (**GIC**), respectively. In accordance with the proposed structure, fragments 532.146 and 502.135 *m/z* can undergo an **I** (-195.053 Da) or **G** (-162.053 Da) losses, resulting in 337.093 (**FG**) or 340.083 *m/z* (**IC**), respectively.

The base peak chromatogram of *m/z* 680.183 $[M-H]^-$ reveals two peaks eluting at rt 7.26 and 7.82 min. The compound eluting at rt 7.26 min is identified as **glu-ind-caff-glu**, or **GIAG**. Fragment 356.078 *m/z* (**IA**) undergoes the usual fragmentation as described earlier for **GIA**. The molecular ion initially cleaves either of the proximal **G**, transition 680.183 → 518.130 *m/z.* The latter is able to cleave another **G** resulting in fragment ions 356.078 (**IA**) *m/z.* The isobar eluting at 7.82 min was identified as **glu-glu-ind-caff**, or **GGIA**. The molecular ion initially cleaves the **A** (-162.032 Da), transition 680.183 → 518.151 *m/z* (**GGI**). In contrary to its isobar **GIAG**, here, **GGIA** demonstrates a loss of **GG** (-324.107 Da) in the transition 680.183 → 356.078 *m/z* (**IA**).

The base peak chromatogram of *m/z* 694.199 $[M-H]^-$ reveals four isobars eluting at rt 5.91, 6.78, 8.05 and 9.64 min. The pair of compounds at rt 5.91 and 9.64 min had identical fragmentation behavior and are identified to have the structure of **glu-glu-ind-fer**, or **GGIF**. Fragment 370.093 *m/z* confirms the **IF**. The **GG** loss appears jointly in the transition 694.199 (**GGIF**) → 370.093 (**IF**) *m/z.* The proximal **F** is cleaved in the transition 694.199 → 518.151 (**GGI**). The proposed structure of the two isobars coincides with oleracein I.

The other isobar pair eluting at 6.77 and 8.04 had identical fragmentation and are identified to have the structure **glu-ind-fer-glu**, or **GIFG**. In contrary to the **GGIF**, here, the neutral losses of each of the proximal **G** (2 × -162.053 Da) appear consecutively in the transitions 694.199 → 532.146 → 370.093 (**IF**) *m/z.* The fragmentation of 370.093 *m/z* is as described for **GIF**. The proposed structure of the two isobars coincides with oleracein D.

The base peak chromatogram of *m/z* 708.193 $[M-H]^-$ reveals two isobars eluting at rt 16.41 and 16.89 min. The eluent at rt 16.41 min, is identified as **sin-glu-ind-coum**, or **SGIC**. Fragment 340.083 *m/z* confirms the **IC**. The molecular ion can cleave consecutively the proximal **C** and then **I** resulting in fragments 562.157 (**SGI**) and 367.103 *m/z* (**SG**), respectively. The latter can cleave a **G**, resulting in 205.051 *m/z* (**S**). The presence of a sinapoyl (**S**) is supported by the neutral loss of 206.054 Da in the transition 708.193 (**SGIC**) → 502.135 *m/z* (**GIC**), as well as the fragments 223.061 and 191.035 *m/z.* The fragmentation of 502.135 *m/z* proceeds as described for **GIC**.

The other isobar eluting at rt 16. 88 min is identified as **fer-glu-ind-fer**, or **FGIF**. Fragment 370.093 *m/z* confirms the **IF**. The molecular ion cleaves a **F**, transition 708.193 → 532.146 *m/z,* followed by either a **G**, or an **I** loss, resulting in fragments 370.093 (**IF**) or 337.093 (**FG**) *m/z,* respectively.

The compound eluting at rt 15.05 min displays a molecular ion at *m/z* 724.189 $[M-H]^-$ and is identified as **sin-glu-ind-caff**, or **SGIA**. Fragment 356.078 *m/z* confirms the **IA**. A neutral loss of the **SG** fragment appears (-368.110 Da) from the molecular ion, transition 724.189 → 356.078 *m/z.* The MS^2 spectra in positive mode was also considered for analysis to further corroborate the proposed structure. The molecular ion at 726.203 $[M+H]^+$ *m/z* cleaves the proximal **A**, followed by an **I** loss to produce fragments 564.173 (1.93) (**SGI**) and 369.117 (6.58) (**SG**) *m/z,* respectively. Fragment ion 358.090 (9.63) *m/z* confirms the **IA**. Fragment ion 369.117 *m/z* (**SG**) can cleave a **G** to produce 207.065 (100) *m/z* (**S**) which can fragment to 147.044 (0.68) *m/z.* **A** is also confirmed with fragment ion 163.038 (45.13) *m/z* and **I** is represented by 196.060 (10.85) *m/z.*

The compound with molecular ion at *m/z* 738.204 $[M-H]^-$, eluting at rt 16.66 min, is identified as **sin-glu-ind-fer**, or **SGIF**. The *N*-feruloyl moiety is confirmed by the fragment at *m/z* 370.093 (**IF**). The molecular ion displays initially either a **F** or **S** (-206.054 Da) loss, resulting in fragments 562.157 (**SGI**) or 532.146 (**GIF**) *m/z,* respectively, although the former is preferred. Fragment 532.146 *m/z* can cleave a **G** resulting in 370.093 *m/z* (**IF**). Fragment ions 223.061 and 205.051 *m/z* corroborate the presence of **S**.

The compound with molecular ion at 784.188 $[M-H]^-$ *m/z* eluting at rt 10.61 min was identified as **hb-glu-glu-ind-coum**, or **OGGIC**. The **IC** fragment is confirmed by the fragment 340.083 *m/z.* The molecular ion can cleave a proximal **C** resulting in fragment 638.173 *m/z* (**OGGI**), which can undergo an **I** loss, resulting in fragment 443.119 *m/z* (**OGG**). The

Preprints (www.preprints.org) | NOT PEER-REVIEWED | Posted: 2 September 2021 doi:10.20944/preprints202109.0048.v1

MS^2 spectra revealed a major peak at *m/z* 137.024 that did not correspond to any previously described in the literature substructure common to oleraceins. Moreover, in the transition 638.173 → 518.151 *m/z* there is a loss of 120.020 Da that suggested a dehydrated derivative of fragment 137.024 *m/z*. This led us to propose that fragment 137.024 *m/z* corresponds to a hydroxybenzoyl moiety (**O**). Fragment 137.024 can cleave a CO_2 to result in fragment 93.033 *m/z* (not shown).

The compound with molecular ion at *m/z* 810.225 $[M-H]^-$ eluting at rt 11.78 min is identified as **coum-glu-glu-ind-coum**, or **CGGIC**. The molecular ion displays initial cleavage of proximal **C**, transition 810.225 → 664.190 *m/z* (**GGIC**). The further fragmentation is identical to that of **GGIC**.

The compound with molecular ion at *m/z* 826.220 $[M-H]^-$ eluting at rt 10.59 min is identified as **caff-glu-glu-ind-coum**, or **AGGIC**. Fragment 340.083 *m/z* confirms the **IC**. The molecular ion can cleave either a **C** or **A**, resulting in fragment ions 680.183 *m/z* (**AGGI**), 664.188 *m/z* (**GGIC**) and 518.151 *m/z* (**GGI**). Fragment 485.130 *m/z* (**AGG**) is also observed. The proposed structure coincides with oleracein K.

The compound with molecular ion at *m/z* 826.241 $[M-H]^-$ eluting at rt 6.34 min is proposed to have the structure of **glu-glu-ind-coum-glu**, or **GGICG**. The molecular ion initially cleaves the single **G**, after which the resulting fragment at 664.188 *m/z* (**GGIC**) can cleave a **C** resulting in 518.151 *m/z* (**GGI**). Fragment 502.135 *m/z* (**ICG**) is formed after a cleavage of the **GG** from the molecular ion. Fragment 518.151 *m/z* also displays **GG** loss resulting in 194.046 *m/z* (**I**). The proposed structure coincides with oleracein P.

The base peak chromatogram of 840.236 $[M-H]^-$ *m/z* reveals five isobars eluting at rt 10.17, 11.95, 12.36, 13.31 and 14.09 min. Except the eluent at rt 13.35 min, all other isobars demonstrated identical fragmentation and are identified

s **fer-glu-glu-ind-coum**, or **FGGIC**, which coincide with the structure of oleracein N or S. Fragment ion 340.083 *m/z* confirms the **IC**. The molecular ion is able to cleave either the proximal **C** or **F** resulting in the transition 840.236 → (694.199 or 664.188) → 518.151 *m/z* (**GGI**). The latter can cleave the **GG** resulting in 194.046 *m/z* (**I**). Fragment 694.199 (**FGGI**) is able to cleave an **I** resulting in fragment ion 499.146 *m/z* (**FGG**). The proposed structure for the isobar eluting at 13.32 is **fer-glu-ind-coum-glu**, or **FGICG**. Initially, the molecular ion cleaves the proximal **G** to produce 678.183 *m/z* (**FGIC**), which can either cleave a **C** or **F**, to produce 532.146 (**FGI**) and 502.135 *m/z* (**GIC**), respectively. The **FGI** fragment ion at 532.146 *m/z* can in turn lose an **I**, resulting in 337.093 *m/z* (**FG**), whereas fragment 502.135 *m/z* (**GIC**) can lose a **C**, resulting in 340.083 *m/z* (**IC**).

The compound with molecular ion at *m/z* 842.215 $[M-H]^-$, eluting at rt 9.34 min, is proposed to have the structure of **caff-glu-glu-ind-caff**, or **AGGIA**. The molecular ion initially cleaves either of its two proximal caffeoyls, to give 680.183 *m/z*. If the *N*-caffeoyl is cleaved, then the **I** can be cleaved (-195.053 Da), resulting in fragment ion 485.130 *m/z* (**AGG**). Fragment 518.151 *m/z* (**GGI**) occurs when both proximal **A** are cleaved. In the other fragmentation pathway, where the initially cleaved caffeoyl is the one linked to **GG**, the stripped hexoses can be cleaved in concert from fragment 680.183 *m/z*, to give fragment 356.078 *m/z* (**IA**).

The compound with molecular ion at *m/z* 842.236 $[M-H]^-$, eluting at rt 6.37 min is proposed to have the structure of **glu-glu-ind-caff-glu**, or **GGIAG**. Fragment 356.078 *m/z* confirms the **IA**. Fragment ion 680.183 *m/z* (**GGIA**) is produced by the cleavage of the proximal **G** from the molecular ion. Fragment ion 518.145 *m/z* is actually composed of two closely *m/z* spaced fragment ions: 518.130 *m/z* (**GIA**) and 518.151 *m/z* (**GGI**). The overlapping of these fragment ions results in the appearance of the 518.145 *m/z*. Fragment ion 518.130 *m/z* results from **GG** cleavage (-324.107 Da) from the molecular ion, and 518.151 *m/z* occurs after consecutive cleavage of the single proximal **G** followed by the **A** cleavage (-324.085 Da total).

The base peak chromatogram of 856.231 $[M-H]^-$ *m/z* reveals three isobars eluting at rt 10.68 and 11.08 min. The compound eluting at rt 10.68 min is identified as **fer-glu-glu-ind-caff**, or **FGGIA**. Fragment 356.078 *m/z* confirms the **IA**. The molecular ion displays a cleavage of proximal **A**, resulting in fragments 694.199 *m/z* (**FGGI**). The latter can cleave

Preprints (www.preprints.org) | NOT PEER-REVIEWED | Posted: 2 September 2021 doi:10.20944/preprints202109.0048.v1

the proximal **F** to result in 518.151 *m/z* (**GGI**), which in turn, after cleavage of **GG,** results in **I** at *m/z* 194.046 *m/z.* The proposed structure coincides with oleracein J. The isobar eluting at rt 11.08 min is identified as **caff-glu-glu-ind-fer**, or **AGGIF**. Fragment 370.093 *m/z* confirms the **IF**. The molecular ion displays consecutive cleavages of **F** and **A**, irrespective of the order, resulting from the transitions 856.231 → (694.199 or 680.183) → 518.151 *m/z* (**GGI**). Fragment 680.183 *m/z* (**AGGI**) can cleave an **I**, resulting in 485.130 *m/z* (**AGG**). Moreover, the latter can cleave **GG**, resulting in fragment at *m/z* 161.024 *m/z* (**A**). The proposed structure coincides with oleracein L.

The base peak chromatogram of 856.252 $[M-H]^-$ *m/z*, eluting at rt 7.04 min is identified as **glu-glu-ind-fer-glu**, or **GGIFG**. Fragment at 370.093 *m/z* confirms the **IF**. The molecular ion can cleave the single **G** to result in fragment 694.199 *m/z* (**GGIF**) that, in turn, can cleave a **F** to result in fragment 518.151 *m/z* (**GGI**). Fragment 532.146 *m/z* (**GIF**) is formed after the **GG** loss from the molecular ion. The proposed structure coincides with oleracein Q.

The base peak chromatogram of 870.246 $[M-H]^-$ *m/z* reveals eight isobars eluting at rt 10.65, 11.71, 12.40, 12.79, 13.20, 13.52, 13.98 and 14.33 min. The isobars eluting at rt 10.65, 12.40 and 12.79 min have identical MS^2 fragmentation and are identified as **fer-glu-glu-ind-fer**, or **FGGIF**. Fragment at *m/z* 370.093 confirms the **IF**. The molecular ion cleaves a proximal **F** resulting fragment 694.199 *m/z* which can either cleave the other **F**, or an **I**, resulting in fragments 518.151 (**GGI**) or 499.146 *m/z* (**FGG**). Both these fragments possess proximal **GG** that can be cleaved, resulting in fragments 194.046 (**I**) and 175.040 *m/z* (**F**), respectively. The proposed structure coincides with oleracein O. The isobars eluting at rt 13.52 and 14.33 min have identical MS^2 fragmentation and are identified as **glu-fer-glu-ind-fer**, or **GFGIF**. Fragment at *m/z* 370.093 confirms the **IF**. Initially, the molecular ion cleaves a **G** resulting in fragment 708.193 *m/z* (**FGIF**). The latter can cleave either of the proximal **F** giving fragment 532.146 *m/z.* Depending on the feruloyl cleaved, the latter fragment can either cleave an **I** or a **G**, resulting in fragments 337.093 (**FG**) or 370.093 *m/z* (**IF**), respectively. The isobars eluting at rt 11.71 and 13.98 min have identical MS^2 fragmentation and are identified as **sin-glu-glu-ind-coum**, or **SGGIC**. Fragment 340.083 *m/z* confirms the **IC**. The molecular ion is able to cleave either **C** or **S**, resulting in the transitions 870.246 → (724.209 (**SGGI**) or 664.188 (**GGIC**)) → 518.151 *m/z* (**GGI**). The latter fragment can cleave the **GG**, resulting in fragment 194.046 *m/z* (**I**). The proposed structure matches oleracein M.

The isobar eluting at rt 13.20 min is identified as **sin-glu-ind-coum-glu**, or **SGICG**. Fragment 340.083 *m/z* confirms the **IC**. The molecular ion exhibits a proximal **G** cleavage, resulting in fragment 708.193 *m/z* (**SGIC**), which in turn can cleave either a **C** or a **S**, resulting in fragments 562.157 (**SGI**) or 502.135 *m/z* (**GIC**), respectively. Fragment 562.157 *m/z* (**SGI**) can cleave the stripped **I** resulting in 367.103 *m/z* (**SG**).

The compound eluting at rt 10.43 min displays a molecular ion at 886.241 $[M-H]^-$ *m/z* and is identified as **sin-glu-glu-ind-caff**, or **SGGIA**. Fragment 356.078 *m/z* confirms the **IA**. The molecular ion exhibits a proximal **A** cleavage resulting in fragment 724.209 *m/z* (**SGGI**). The latter can either cleave an **I** or a **S**, resulting in fragments 529.156 (**SGG**) or 518.151 *m/z* (**GGI**), respectively. Both these fragments can lose the proximal **GG** in concert resulting in a **S** (202.051 m/z) or an **I** (194.046 m/z) fragment ions.

The base peak chromatogram of 900.256 $[M-H]^-$ *m/z* reveals four isobars eluting at rt 10.56, 12.12, 13.41 and 14.09 min. All compounds but the eluent at rt 13.41 min showed identical fragmentation and are identified as **sin-glu-glu-ind-fer**, or **SGGIF**. The molecular ion is able to cleave either proximal **F** or **S** resulting in the transitions 900.256 → (724.209 (**SGGI**) or 694.199 (**GGIF**)) → 518.151 *m/z* (**GGI**). Fragment 724.209 *m/z* can lose the stripped **I** resulting in fragment at 529.156 *m/z* (**SGG**). Fragment 529.156 and 518.151 *m/z* can both cleave their **GG** resulting in fragments 205.051 (**S**) or 194.046 *m/z* (**I**). The proposed structure matches oleracein X.

The isobar eluting at rt 13.41 min is identified as **glu-sin-glu-ind-fer**, or **GSGIF**. Fragment at *m/z* 370.093 confirms the **IF**. After the proximal **G** cleavage from the molecular ion, the resultant fragment at 738.205 *m/z* (**SGIF**) is able to cleave either **F** or **S**, resulting

Preprints (www.preprints.org) | NOT PEER-REVIEWED | Posted: 2 September 2021 doi:10.20944/preprints202109.0048.v1

in fragments 562.157 (**SGI**) and 532.146 *m/z* (**GIF**), respectively. Fragment 562.157 *m/z* can lose the **I** resulting in fragment 367.103 *m/z* (**SG**) which in turn can lose a **G** to give the **S** fragment featured at 205.051 *m/z*. Fragment 532.146 *m/z* can lose the proximal **G** to give fragment 370.093 *m/z* (**IF**).

The compound eluting at rt 8.65 min having a molecular ion at 946.262 $[M-H]^-$ *m/z* is identified as **hb-glu-glu-ind-coum-glu**, or **OGGICG**. Fragment at *m/z* 340.083 confirms the **IC**. The molecular ion initially cleaves the single **G** to give fragment 784.215 *m/z* (**OGGIC**) which in turn can lose a **C** to give fragment 638.173 *m/z* (**OGGI**). The latter can lose an **I** to result in 443.119 *m/z* (**OGG**). Fragment 638.173 *m/z* can also lose a hydroxybenzoyl moiety (**O**) (-120.020 Da) to result in 518.151 *m/z* (**GGI**). The latter can cleave **GG** to result in 194.046 *m/z* (**I**). Similar to oleracein **OGGIC** described before, here we observe fragment ion 137.024 *m/z* (**O**). The decarboxylated fragment of 137.024 *m/z* is also observed at 93.033 *m/z* (not shown). The MS^2 data in positive ionization mode shows a dehydrated hydroxybenzoyl derived fragment ion at 121.029 *m/z*.

The base peak chromatogram of 988.273 $[M-H]^-$ *m/z* reveals four isobars eluting at rt 7.78, 8.52, 9.45 and 10.07 min. The compound eluting at 7.78 min is identified as **caff-glu-glu-ind-coum-glu**, or **AGGICG**. Fragment at *m/z* 340.083 confirms the **IC**. Initially, the molecular ion is observed to make the transition 988.273 → 826.241 *m/z* (-162.045 Da), where the difference of 162.045 Da is a weighted average of either a **G** (-162.053 Da) or **A** (-162.032 Da) loss. Accordingly, the abovementioned fragment ion 826.220 *m/z* is a weighted average of 826.220 (**AGGIC**) and 826.241 *m/z* (**GGICG**). Afterwards, 664.188 *m/z* (**GGIC**) fragment ion is observed. Fragment 680.183 *m/z* (**AGGI**) results from consecutive **G** and **C** losses from the molecular ion and is able to cleave the stripped **I** to produce 485.130 *m/z* (**AGG**). Fragment 664.188 *m/z* as well as 485.130 *m/z* both possess proximal **GG** that can be cleaved in concert, resulting in 340.083 (**IC**) and 161.024 *m/z* (**A**), respectively. The isobars eluting at rt 8.52 and 9.45 min demonstrate identical fragmentation behavior and are identified as **glu-caff-glu-glu-ind-coum**, or **GAGGIC**. Fragment ion 340.083 *m/z* confirms the **IC**. The molecular ion can lose a **C** and **G** resulting in the transitions 988.273 → (842.236 or 826.220) → 680.183 *m/z* (**AGGI**). Fragment ion 826.220 *m/z* (**AGGIC**) can lose the **A** to result in 664.188 *m/z* (**GGIC**). Fragment ion 680.183 *m/z* can cleave **A** or **I** resulting in 518.151 (**GGI**) or 485.130 *m/z* (**AGG**), respectively. The latter two fragments can both cleave **GG** to result in fragment ions 194.046 (**I**) and 161.024 (**A**) *m/z*, respectively. The isobar eluting at rt 10.07 min is identified as **caff-glu-glu-glu-ind-coum**, or **AGGGIC**. Fragment ion 340.083 *m/z* confirms the **IC**. The molecular ion can lose the proximal **C** or **A** resulting in the transitions 988.273 → (842.236 or 826.241) → 680.204 *m/z* (**GGGI**). Here, the three hexoses are conjoint, and thus, their cleavage is observed in concert (-486.159 Da) from fragment 680.204 *m/z*, resulting in 194.046 *m/z* (**I**). Accordingly, fragment 826.241 *m/z* (**GGGIC**) also demonstrates the potential of the **GGG** loss, transition 826.241 → 340.083 *m/z* (**IC**).

The base peak chromatogram of 988.294 $[M-H]^-$ *m/z* reveals three isobars eluting at rt 5.83, 6.03 and 6.21 min. The compound eluting at rt 5.83 min is identified as **glu-glu-ind-coum-glu-glu**, **GGICGG**. Fragment 340.083 *m/z* confirms the **IC**. In accordance with the proposed structure, the molecular ion can cleave **GG** on either side of the molecule, resulting in the transitions 988.294 → 664.188 → 340.083 *m/z* (**IC**). If the cleaved **GG** are linked to the coumaroyl, the **C** is observed to be cleaved, resulting in the transition 664.188 → 518.151 *m/z* (**GGI**). The latter can cleave **GG** to result in fragment 194.046 *m/z* (**I**). The isobars, eluting at rt 6.03 and 6.22 min, display identical fragmentation and are identified as **glu-glu- glu-ind-coum-glu**, or **GGGICG**. Fragment ion 340.083 *m/z* confirms the **IC**. The transition 988.294 → 826.241 (**GGGIC**) → 680.204 *m/z* (**GGGI**) corresponds to consecutive losses of the proximal single **G** followed by a **C** loss from the molecular ion. The loss of the **GGG** is observed in the transition 988.294 → 502.135 *m/z* (**ICG**) as well in the transition 680.204 → 194.046 *m/z* (**I**). Then fragment 502.135 *m/z* (**ICG**) can lose the other **G** to result in 340.083 *m/z* (**IC**).

Preprints (www.preprints.org) | NOT PEER-REVIEWED | Posted: 2 September 2021 doi:10.20944/preprints202109.0048.v1

Diagnostic ions

Since oleracein compounds bear similar structure, we sought to refine the "fragment ion pool" and to select diagnostic fragment ions that can be used to describe the identified oleraceins. And so, after thorough MS^2 fragmentation analysis of the identified 51 oleraceins, we selected 43 fragment ions, their elemental compositions and exact masses determined, that were utilized as diagnostic ions for the identified substances. Hence, each oleracein could be described as a vector of length 43 with values equal to the relative intensities of the corresponding diagnostic ions. A fragment ion from an MS^2 data of a particular oleracein was assigned to a diagnostic ion if its *m/z* were within 15 ppm error of the diagnostic ion's *m/z*. All diagnostic ions had the following features: a mass greater than 100 Da, were encountered in 2 or more oleraceins, had a mean percent intensity greater than 5%, and a maximum percent intensity greater than 10%. The diagnostic fragment ions along with their featured structures are shown in Table S4 and discussed below in increasing mass.

Fragment ion 137.0243 *m/z* is derived from the hydroxybenzoyl (**O**) moiety, as described in the identification of **OGGIC** and **OGGICG**. The coumaroyl (**C**) moiety can be evident by the fragment ion at 145.0294 *m/z*. The caffeoyl (**A**) can be confirmed with fragment ion 161.0243 *m/z*, however, if not linked to the indoline core (**I**), fragment 179.0349 *m/z* may as well be present. Fragment 161.0243 *m/z* might indicate a feruloyl (**F**) as well, however, in our study, the caffeoyl produced > 60%, whereas the feruloyl produced < 30% intensity of fragment ion 161.0243 *m/z*. Fragment ion 175.0400 *m/z* indicates the presence of **F**. The appearance of fragment 193.0506 *m/z* might indicate **F** not linked to **I**. The **I** is featured by fragment ions 194.0458, 150.0560 and 148.0403 *m/z*, in decreasing intensity. Fragment 194.0458 *m/z* as well as the characteristic fragments for the HCAs are usually very prominent, their intensity decreases with increasing the mass of the molecule, unless the molecule possesses easily cleavable moieties, like consecutive glucopyranoses, as in **GGGICG** or **GGICGG**. Fragment 205.0505 *m/z* is observed in all identified substances, bearing the sinapoyl (**S**) moiety, as well as fragment 223.0611 *m/z*, in lower intensity. As the **S** is encountered only linked to a glucopyranosyl (**G**), fragment ions 562.1565 and 367.1034 *m/z* corresponding to the **SGI** and **SG** substructures, respectively, can indicate the presence of **S**.

As mentioned above, the ind-HCA structures **IC**, **IA** and **IF** are confirmed with their corresponding fragment ions: 340.0826, 356.0775 and 370.0931 *m/z*, respectively. However, as the mass of the oleracein increases, the intensities of these characteristic fragments might lower. If the oleraceins bear easily cleavable moieties, like two or three consecutively linked **G**, the fragment ions indicating the ind-HCA structures may be more prominent. Thus, in the oleracein **GGGICG**, where the **GGG** cleave together as a neutral loss of 486.159 Da, high intensity of fragment 340.0826 *m/z* (64%) is observed, as well as fragment 145.0294 *m/z* (100%). On the other hand, in the oleracein **AGGIC**, lower intensities of both these fragments are observed (11% and 37%, respectively).

The **IC** fragment at 340.0826 *m/z* undergoes consecutive CO_2 and CO cleavages, resulting in fragments 296.0927 and 268.0978 *m/z*, respectively, in decreasing intensity. The same fragmentation behavior is established for the **IF** fragment at 370.0931 *m/z*, where the transition 370.0931 → 326.1033 → 298.1084 *m/z* is observed. The fragmentation of **IA** at 356.0775 *m/z*, however, is somewhat different. Very little if any of the CO_2 and then CO losses could be observed from the **IA** fragment. Instead, 356.0775 *m/z* loses $C_6H_6O_2$ (-110.036 Da), which corresponds to the dihydroxybenzene moiety from the caffeoyl. Additionally, the dihydroxybenzene fragment could be confirmed at 109.0295 *m/z*. The resultant fragment at 246.0407 *m/z* then loses CO_2 to produce fragment 202.0509 *m/z*. And so, in **IA**, the transition 356.0775 → 246.0407 → 202.0509 *m/z* is established, and the intensities are higher than the abovementioned daughter fragment ions for **IC** and **IF**. The rest of the diagnostic ions and their features are listed in Table S4.

Preprints (www.preprints.org) | NOT PEER-REVIEWED | Posted: 2 September 2021 doi:10.20944/preprints202109.0048.v1

2.2. Clustering methods

The clustering methods express similarity of the oleraceins based on their MS^2 features. Initially, a *m* by *n* ions matrix was created describing every oleracein (rows, $m = 51$) with their corresponding diagnostic ions (columns, $n = 43$), shown in Table S5. Every cell in the matrix represents the percentage intensity of a diagnostic ion for a particular oleracein. If a diagnostic ion was missing in the MS^2 data of a compound, zero intensity was assigned. This data was imported to RStudio and manipulated further with the R programming language. Different methods were used to cluster the oleraceins based on their MS^2 features. As a primary step, a distance matrix was created (51×51), calculating the euclidean distance from the ions matrix. Figure 4 represents the ordered and unordered heatmaps, using the data from the distance matrix.

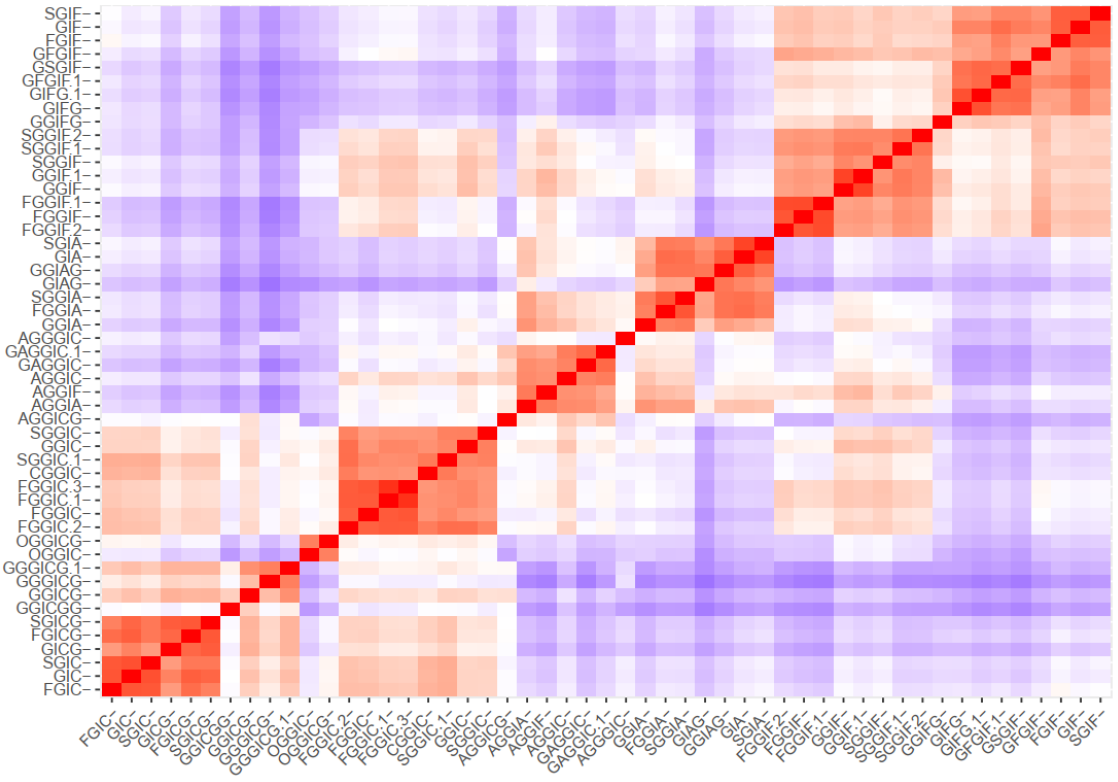

Preprints (www.preprints.org) | NOT PEER-REVIEWED | Posted: 2 September 2021 doi:10.20944/preprints202109.0048.v1

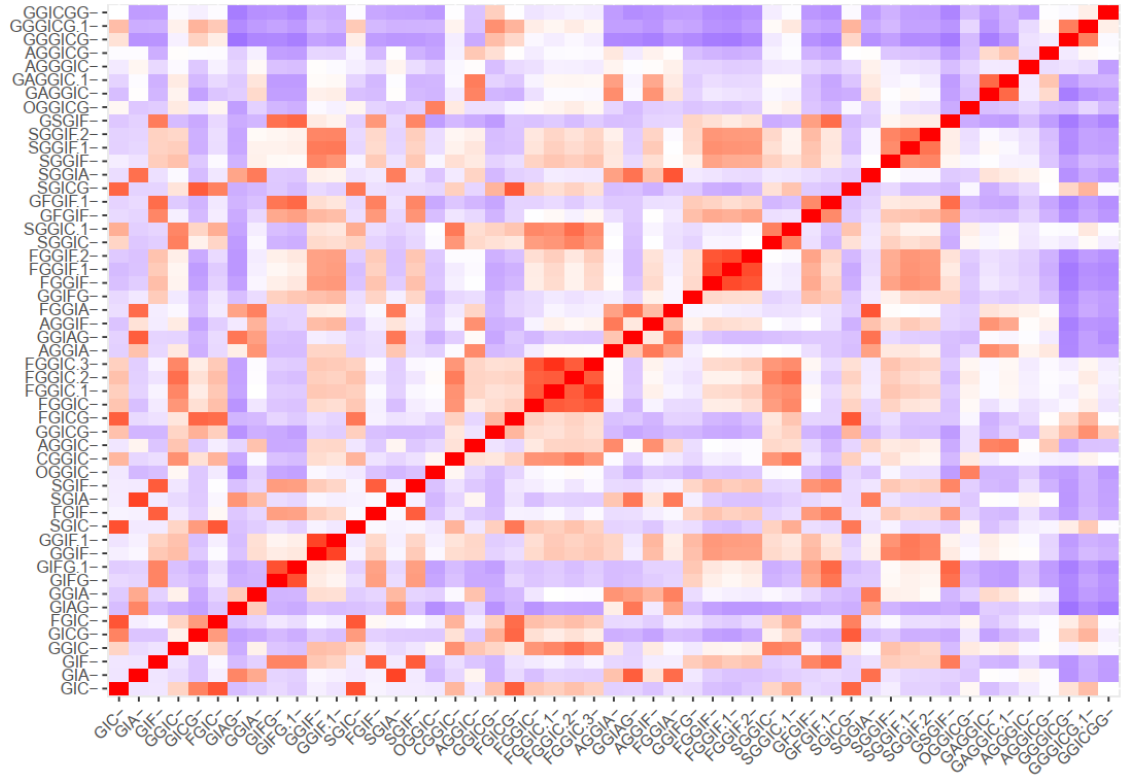

Figure 4. Ordered and unordered heatmaps based on a distance matrix using the MS² data of the 51 identified oleracein (red – higher and blue – lower value).

Then, *k*-means and pam clustering were used to estimate the optimal number of clusters. The clustering observed in the ordered heatmap (Figure 4), as well as the data of the *k*-means and pam clustering (supplementary material Figure S1 and Figure S2), gave us grounds to cluster our data with 8 clusters (Figure 5). Distribution of individuals in the groups can be found in Table S6.

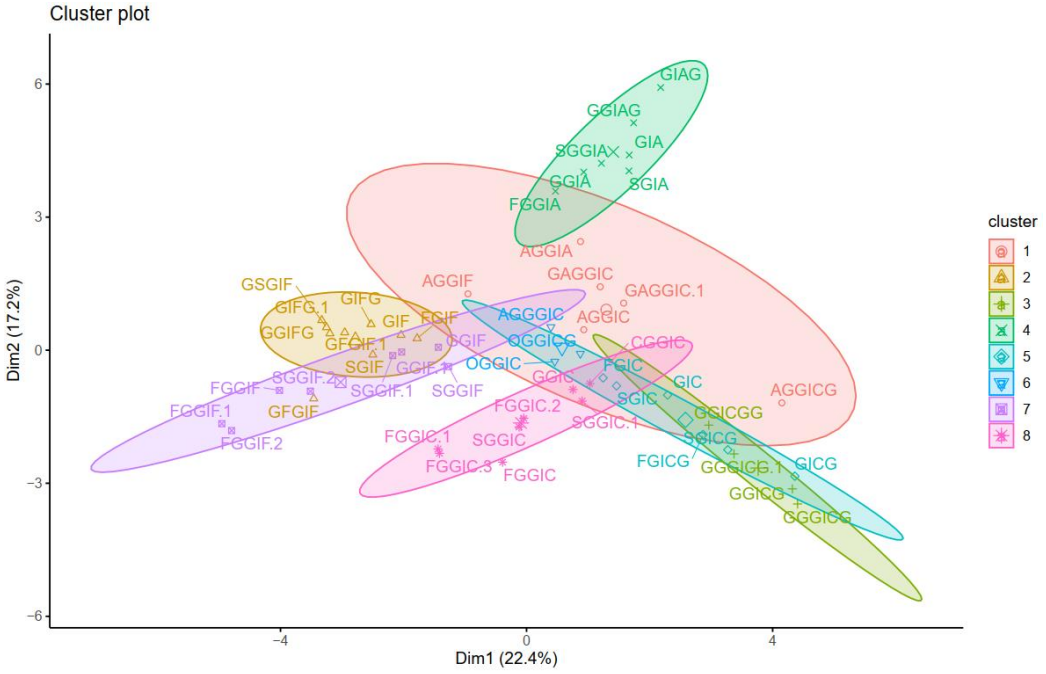

Figure 5. Visualization of the *k*-means clustering.

Preprints (www.preprints.org) | NOT PEER-REVIEWED | Posted: 2 September 2021 doi:10.20944/preprints202109.0048.v1

Next, principal components were calculated. Scree plot (representing the percentage of variances explained by each principal component) can be found in Figure S3. The PCA visualization is presented in Figure 6, where the color gradient from orange (darker) to blue (lighter) presents the quality of representation (cos2), from high to low. A high cos2 indicates a good representation of the variable on the principal component, and *vice versa*. Hence, regarding the well represented oleraceins, three groups can be distinguished, that are characterized with either **IA** (1st quadrant), **IF** (2nd quadrant) or **IC** (4th quadrant) sub-structures. The quality of representation (cos2) of individuals as well as a visualization of the contribution of individuals on PC1 and PC2 are given in Figure S4 and Figure S5.

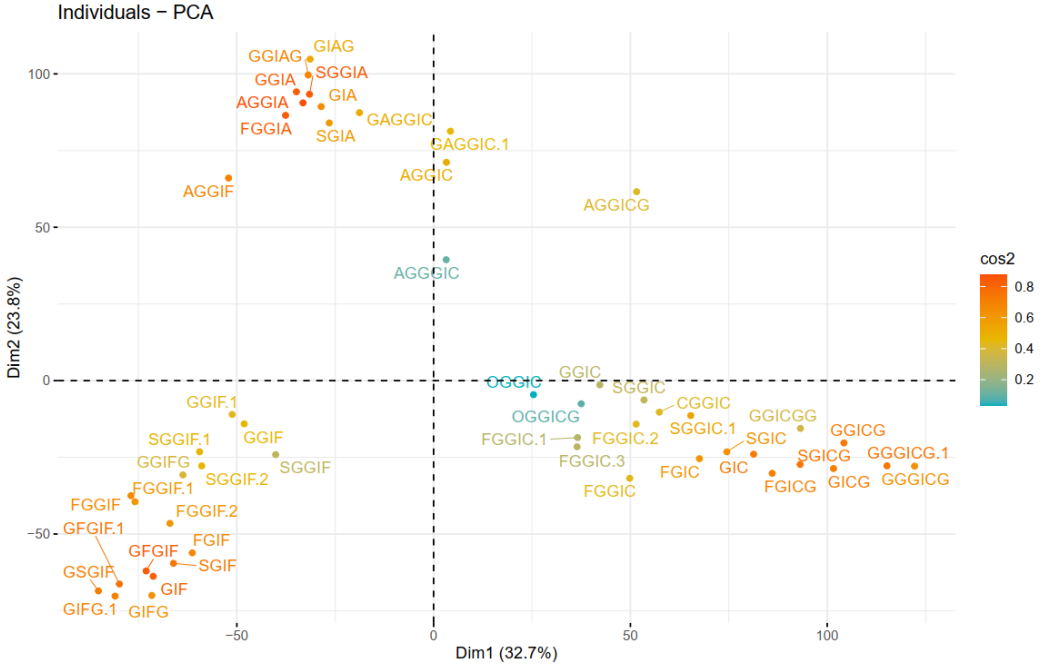

Figure 6. PCA plot of individuals (oleraceins).

Figure 7 depicts the clustering of the individual fragment ions, positively correlated variables (fragment ions) point to the same side of the plot, and *vice versa*. Thus, we can clearly observe which fragment ions "go together" (are parent ion → daughter ion). As expected, identical to Figure 6, the fragment ions corresponding to **IA** (1st quadrant), **IF** (2nd quadrant) and **IC** (4th quadrant), are observed as they are described in the "Diagnostic ions" section and presented in Figure 2.

Preprints (www.preprints.org) | NOT PEER-REVIEWED | Posted: 2 September 2021 doi:10.20944/preprints202109.0048.v1

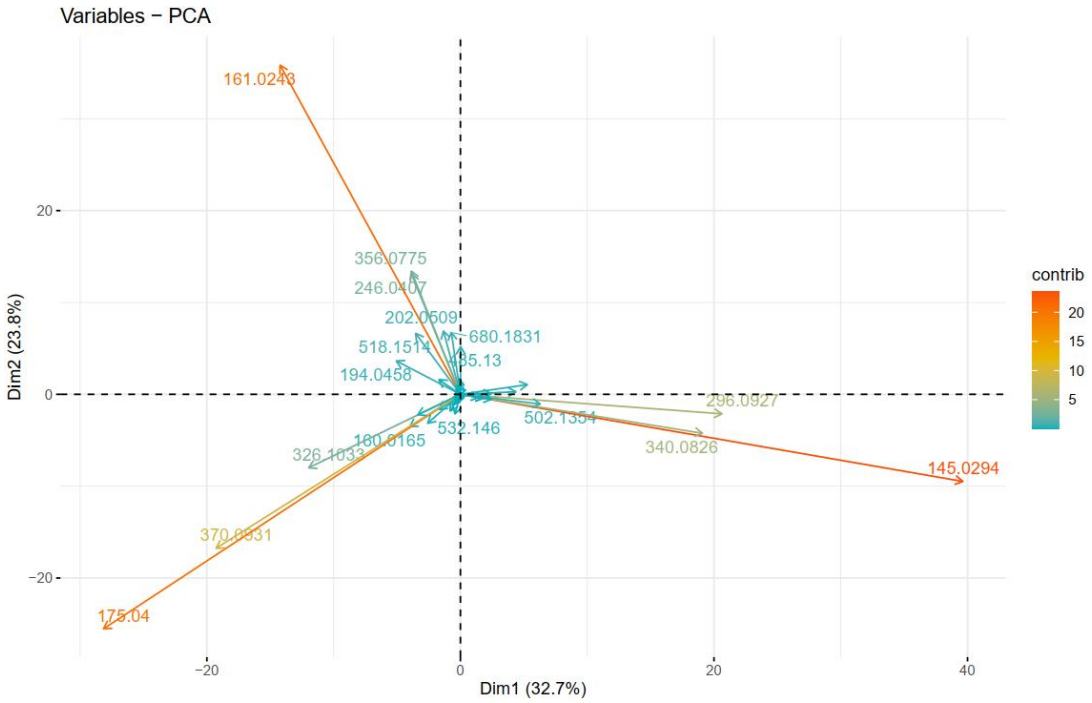

Figure 7. PCA plot of variables (fragment ions).

Next, hierarchical clustering was employed with method = "average". The cophenetic correlation coefficient was calculated to be 0.85. The hierarchical clustering is visualized as a dendrogram and a phylogenetic tree in Figure 8, where the tree was "cut" into 8 parts.

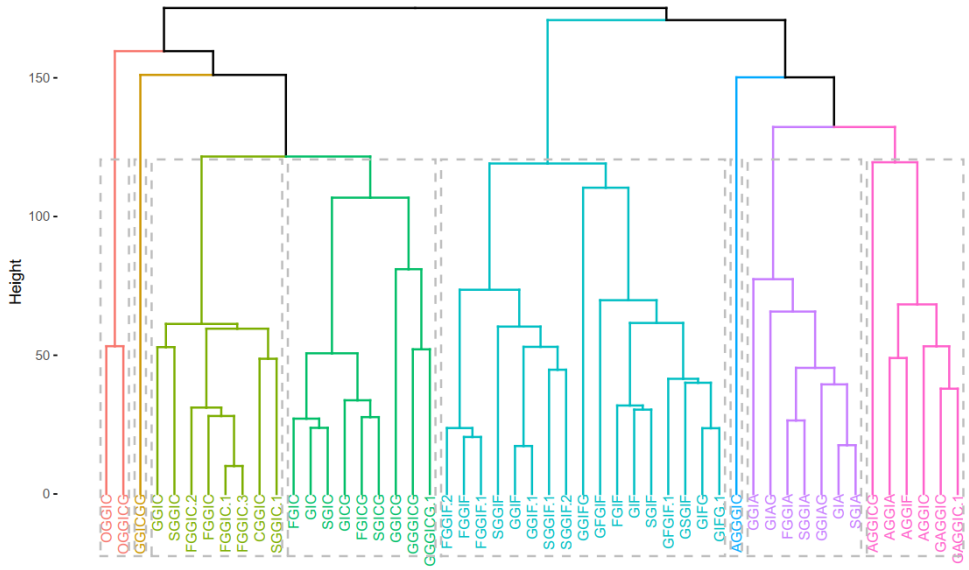

Preprints (www.preprints.org) | NOT PEER-REVIEWED | Posted: 2 September 2021 doi:10.20944/preprints202109.0048.v1

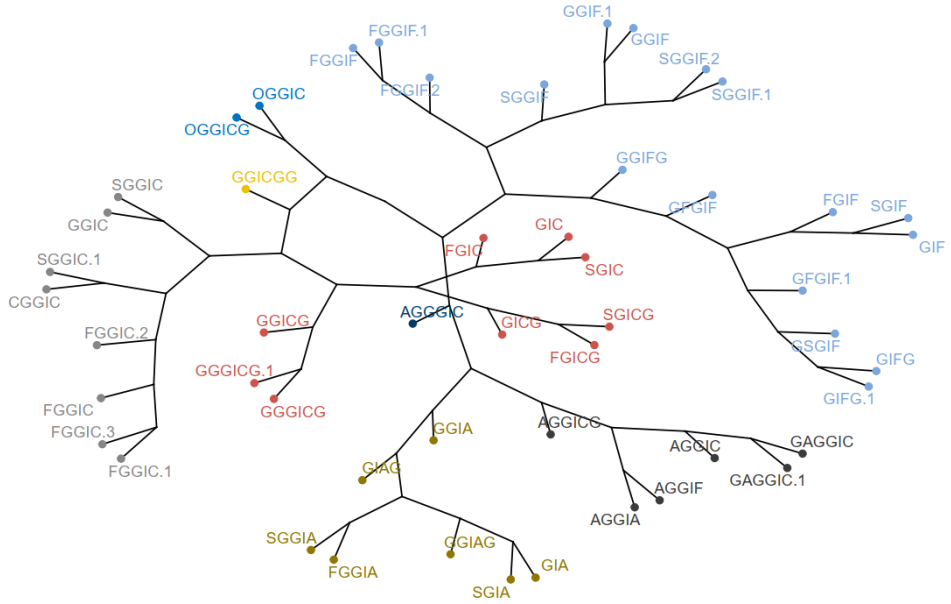

Figure 8. Dendrogram (upper) and phylogenetic tree - like dendrogram (lower) of the 51identified oleraceins.

Overall, the different clustering methods used give very similar clustering. In accordance with the proposed structures, different isoforms with the same structure are clustered together. In general, oleraceins are grouped depending on the presence of either of the three common substructures: **GIC**, **GIA**, or **GIF** that give rise to other diagnostic fragment ions. Thenceforward, different combinations or permutations of substructures lead to specific diagnostic fragment ions.

Oleraceins **GIC**, **FGIC**, **SGIC**, **GICG**, **FGICG** and **SGICG** have either **GIC** or **GICG** in common and are grouped together. Next, **GGICGG** has the unique feature that there is a **GG** attached to the *N*-coumaroyl. It does, however, show some similarity to **GGICG**, **GGGICG**, **GGGICG.1.** The latter three cluster together, because of the **ICG** substructure. Next, a cluster composed of **GGIC**, **CGGIC**, **FGGIC**, **FGGIC.1**, **FGGIC.2**, **FGGIC.3**, **SGGIC** and **SGGIC.1** is formed with the **GGIC** as a common feature, and no **G** attached to the *N*-coumaroyl. The two representatives possessing **O** are clustered together; fragment ion 137.0243 *m*/*z* corresponding to the **O** substructure is exhibited at high intensity and unique to **OGGIC** and **OGGICG**. Oleracein **AGGICG** shows uniqueness due to a proximal **A**, as well as there is a **G** attached to the *N*-coumaroyl. Oleracein **AGGICG** demonstrates greater similarity with **AGGIC**, **GAGGIC** and **GAGGIC.1**, which conforms with their proposed structures. Another cluster comprised of **AGGIA**, **AGGIF**, **AGGIC**, **GAGGIC** and **GAGGIC.1** is formed with the **AGGI** substructure in common. The **A** not attached to **I** is indicated by the appearance of fragment ion 179.035 *m*/*z*, in addition to 161.0243 *m*/*z*, characteristic for **A**. Moreover, fragment ion 680.1831 *m*/*z*, that indicates **GGIA** or **GIAG** or **AGGI**, is exhibited in prominent intensity. **AGGGIC** shows distinctive MS^2 features due to, on one hand, the proximal **A**, and on the other hand, the **GGG**. Other clustered oleraceins bearing the **GIA** substructure include: **GGIA**, **FGGIA** and **SGGIA** with the **GGIA** substructure in common. **GIAG** and **GGIAG,** as well as **GIA** and **SGIA,** are clustered pairs, which is also evident from their structures. Oleraceins **FGGIF**, **FGGIF.1**, **FGGIF.2**, **GGIF**, **GGIF.1**, **SGGIF**, **SGGIF.1**, and **SGGIF.2** are grouped with **GGIF** as a common substructure. Another grouping is formed between oleraceins with the **GIFG** substructure, namely **GIFG**, **GGIFG** and **GIFG.1**. The rest of the oleraceins bearing the **GIF** do not possess **G** attached to the *N*-feruloyl, have a single **G** attached to **I**, and not **GG** or **GGG**. They are grouped and represented with oleraceins **GIF**, **FGIF**, **GFGIF** and **SGIF**.

 doi:10.20944/preprints202109.0048.v1

Worth mentioning is that the calculated similarities cannot provide direct quantitative measure of the structural similarity. Some substructures (or moieties) are represented with more than one diagnostic fragment ion, and others are not. Additionally, some diagnostic fragment ions exhibit, in general, higher intensity than others. Nevertheless, the clustering analysis performed by us demonstrates that this approach can provide additional perception on the relationships of MS^2 fragment ions and outline groups of parent ion → daughter ion.

3. Conclusions

Herein, utilizing UHPLC-Orbitrap-HRMS technique, a total of 51 oleraceins were tentatively identified in hydromethanolic extracts of purslane, 25 of them are new structures. Diagnostic ion filtering (DIF) and diagnostic difference filtering (DDF) were employed to filter out MS data. Moreover, all 51 identified oleraceins were represented with a selected set of 43 diagnostic fragment ions that permitted the generation of a distance matrix. Furthermore, clustering of the identified oleraceins, based on their MS^2 features, was achieved, and presented by heatmaps, pam and *k*-means clustering, principal component analysis and hierarchical clustering. Here, we demonstrate that clustering methods can provide valuable insights in the MS^2 elucidation of natural compounds in complex mixtures.

4. Materials and Methods

4.1. Plant material

Portulaca oleracea, L. aerial parts were gathered from v. Orizovo, Bulgaria (42.208889° N -25.170278° E) and identified by one of us (V.B.). Voucher specimens were deposited at the Faculty of Pharmacy, Medical University, Sofia, Bulgaria (Herbarium Facultatis Pharmaceuticae Sophiensis № 1563-1574).

4.2. Extraction and sample preparation

The hydromethanolic extracts of purslane were obtained as described in our previous study [28]. In brief, air-dried aerial parts of purslane were powdered, and 3.00 g of plant material were extracted twice by sonication with 10 ml 50% MeOH at 50 °C for 15 min in an ultrasonic bath. The combined extracts were filtered and diluted to 25 ml in volumetric flasks with 50% MeOH. The solutions were filtered through a 0.22 μm syringe filter, and 1μL was injected into the LC instrument for LC-MS analysis.

4.3. UHPLC-HR-MS instrument

The UHPLC system consisted of Dionex UltiMate 3000 RSLC HPLC, equipped withan SRD-3600 solvent rack degasser, an HPG-3400RS binary pumpwith solvent selection valve, a WPS-3000TRS thermostated autosampler, and a TCC-3000RS thermostated column compartment (Thermo Fisher Scientific). The UHPLC system was controlled by Chromeleon software, version 7.2. The effluents were connected on-line with a Q Exactive Plus mass spectrometer (Thermo Fisher Scientific) equipped with a heated electrospray ionization (HESI-II) probe.

4.4. Chromatographic parameters

Elution was carried out on Kromasil EternityXT C18 (1.8 μm, 2.1×100 mm) column maintained at 40 °C. The chromatographic conditions were as described elsewhere [28] with slight modifications. The binary mobile phase consisted of A: 0.1% formic acid in water, and B: 0.1% formic acid in acetonitrile. The total run time was 23.5 min. The acquisition time where substances were analyzed with MS was 19 min and set between the 1st and the 20th min. The following gradient was used: the mobile phase was held at 5% B for 0.5 min and then gradually turned to 33% B over 19.5 min. Next, % B was increased gradually to 95 % over 1 min and maintained at 95% B for 2 min. The system was turned to the initial condition of 5% B in 1 min and re-equilibrated over 4 min. The flow rate and the injection volume were set to 300 μL/min and 1 μL, respectively.

Preprints (www.preprints.org) | NOT PEER-REVIEWED | Posted: 2 September 2021 doi:10.20944/preprints202109.0048.v1

4.5. Mass spectrometric parameters

For MS^2 fragmentation analysis, several normalized collision energies (NCE) were tested to select the optimal conditions. The 20 NCE gave satisfactory abundance of variety of heavier fragment ions, and 40 NCE provided good intensity to lower *m/z* specific fragment ions, and thus, a stepped 20-40 NCE was selected for initial screening of oleraceins. Mass spectrometric parameters for Full-scan MS were as follows: resolution 17,500; AGC target 1e6; Maximum IT 83ms; Scan range 500 – 2000 *m/z*. For dd-MS^2, the following parameters were used: TopN 10; isolation window 1.0 m/z; stepped NCE 20-40; Minimum AGC target 8.00e3; Intensity threshold 9.6e4; Apex trigger 2 to 6 sec; Dynamic exclusion 3 sec. The structural elucidation of the oleraceins was achieved by manual inspection of the MS^2 spectra in Xcalibur 4.2 software (Thermo Fisher Scientific).

4.6. Mass spectral filtering by Diagnostic Ion Filtering (DIF) and Diagnostic Difference Filtering (DDF)

Initially, vendor *.raw (Thermo Fisher Scientific) files were converted to *.mzML files by MSConvertGUI 3.0 (ProteoWizard) and imported to MZmine 2.53. Then, DIF was applied based on the presence of two of the specific fragment ions for 5,6-dihydroxyindoline-2-carboxylic acid (called below in the text as "indoline core"): 194.0459 *m/z* (chemical formula: $C_9H_8O_4N^-$) and 150.0560 *m/z* (chemical formula: $C_8H_8O_2N^-$) (Figure 2), with a ± 15 ppm threshold. MZmine also offers "diagnostic neutral loss" filtering for searching of specific mass difference(s) only between the precursor ion and each of its fragments. However, since we were interested in searching for the specific mass difference including between fragment ions of the same precursor ion (Figure 3), a DDF approach was applied to refine the selection of molecules that supposedly possess the 5,6-dihydroxyindoline-2-carboxylic acid substructure. DDF involved searching for a specific mass difference between each fragment (including the precursor ion, even if it was not present in the MS^2 spectrum) and all lower *m/z* fragment ions. That difference was set to 195.05316 Da that suggested a neutral loss of 5,6-dihydroxyindoline-2-carboxylic acid. DDF was achieved by an in-house script written in Python 3.7.1 programming language. The defined threshold was set to ± 15 ppm of the ions from which the difference originated. Thus, in the fragmentation transition 340.0848 *m/z* → 145.0300 *m/z*, with a threshold of ± 15 ppm, the searched difference was between 145.0300 ± 15 ppm and 340.0848 ± 15 ppm (i.e., from 195.0475 Da to 195.0621 Da). And so, if the difference originated from heavier fragments, a bigger mass threshold was used, and *vice versa*.

4.7. Grouping of MS^2 scans

In order to group MS^2 scans that presumably derive from the same substance, MS^2 scans with precursor ion *m/z* within 15 ppm and within 1.5 % deviation in retention times were added together, and afterwards manually checked. In these grouped MS^2 scans, fragment ions that were within 15 ppm *m/z* were considered identical, their intensities added, and their masses recalculated by weighted mean averaging:

$$(m/z)_{avg} = \frac{\sum_{i=1}^{N} int_i \times (m/z)_i}{N}$$

where $(m/z)_{avg}$ is the recalculated *m/z* value, $(m/z)_i$ and int_i are the *m/z* and the intensity of the i^{th} fragment ion, respectively. Fragment ions having less than 0.5 % intensity and mass < 100 Da were excluded. The retention time of the precursor ion with the highest intensity was chosen as the retention time of grouped MS^2 scans, i.e., the peak apex.

 doi:10.20944/preprints202109.0048.v1

4.8. Clustering methods

Clustering methods including heatmaps, *k*-means and pam clustering, principal component analysis (PCA) and hierarchical clustering were conducted in R 4.1.0 programming language [31] operated under RStudio (Version 1.4.1717, RStudio, PBC). Clustering visualizations were achieved using the package "factoextra" 1.0.7 [32]. Other used R packages include: "tidyverse" 1.3.1 [33], including packages "dplyr" 1.0.7 and "readr" 2.0.0; package "cluster" 2.1.2 [34]; package "igraph" 1.2.6 [35]; package "dendextend" 1.15.1 [36]. Distance matrix and hierarchical clustering were calculated with method = "euclidean" and method = "average", respectively.

4.9. Used abbreviations

For simplicity and clarity of the presentation, the following abbreviations are used throughout this paper: hydroxybenzoyl: hydroxycinnamic acid: HCA ; **hb** or **O**; coumaroyl: **coum** or **C**; caffeoyl: **caff** or **A**; glucopyranosyl: **glu** or **G**; feruloyl: **fer** or **F**; indoline core: **ind** or **I**; sinapoyl: **sin** or **S**. In case multiple oleraceins bore the same structure, the names of the compounds were suffixed with numbers, i.e., **FGGIC**, **FGGIC**.1, **FGGIC**.2, etc. (Table 2 and Table 3).

Supplementary Materials:

The **supplementary tables** are available online at www.mdpi.com/xxx/...

Table S1: Transitions; Table S2: MS2 raw data; Table S3: MS2 Diagnostic ions; Table S4: Diagnostic ions features; Table S5: Ions matrix; Table S6: Cluster groups

The **supplementary figures** are available online at www.mdpi.com/xxx/...

Figure S1: Estimating the optimal number of clusters with *k-means* clustering; Figure S2: Estimating the optimal number of clusters with *pam* clustering; Figure S3: Scree plot representing the percentage of variances explained by each principal component; Figure S4: Visualization of the quality of representation of individuals (cos2); Figure S5: Visualization of the contribution of individuals on PC1 and PC2

Author Contributions: Conceptualization, Y.V. and R.G.; methodology, P.N.; Plant gathering and extract preparation, V.B., R.G and D.Z; software, Y.V. and I.D.; data curation, Y.V; investigation, Y.V. and D.Z; writing—original draft preparation, Y.V.; writing—review and editing D.Z, P.N., I.D.; visualization, Y.V; project administration, Y.V; funding acquisition, Y.V. All authors have read and agreed to the published version of the manuscript.

Funding: Please add: This research was funded by Council of Medical Sciences, Medical University of Sofia, Bulgaria, grant number 123/24.06.2020. The APC were covered by the authors.

Conflicts of Interest: The authors declare no conflict of interest.

References

1. Corrado, Giandomenico, Christophe El-Nakhel, Giulia Graziani, Antonio Pannico, Armando Zarrelli, Paola Giannini, Alberto Ritieni, Stefania De Pascale, Marios C Kyriacou, and Youssef Rouphael. "Productive and Morphometric Traits, Mineral Composition and Secondary Metabolome Components of Borage and Purslane as Underutilized Species for Microgreens Production." *Horticulturae* 7, no. 8 (2021): 211.
2. Melilli, Maria Grazia, Vita Di Stefano, Fabiola Sciacca, Antonella Pagliaro, Rosaria Bognanni, Salvatore Scandurra, Nino Virzì, Carla Gentile, and Massimo Palumbo. "Improvement of Fatty Acid Profile in Durum Wheat Breads Supplemented with Portulaca Oleracea L. Quality Traits of Purslane-Fortified Bread." *Foods* 9, no. 6 (2020): 764.
3. Petropoulos, Spyridon A, Ângela Fernandes, Maria Inês Dias, Ioannis B Vasilakoglou, Konstantinos Petrotos, Lillian Barros, and Isabel CFR Ferreira. "Nutritional Value, Chemical Composition and Cytotoxic Properties of Common Purslane (Portulaca Oleracea L.) in Relation to Harvesting Stage and Plant Part." *Antioxidants* 8, no. 8 (2019): 293.
4. Akbar, Shahid. "Portulaca Oleracea L. (Portulacaceae)." In *Handbook of 200 Medicinal Plants: A Comprehensive Review of Their Traditional Medical Uses and Scientific Justifications*, 1491-504. Cham: Springer International Publishing, 2020.
5. Saffaryazdi, Azadeh, Ali Ganjeali, Reza Farhoosh, and Monireh Cheniany. "Variation in Phenolic Compounds, A-Linolenic Acid and Linoleic Acid Contents and Antioxidant Activity of Purslane (Portulaca Oleracea L.) During Phenological Growth Stages." *Physiology Molecular Biology of Plants* 26, no. 7 (2020): 1519-29.
6. Kumar, Ajay, Sajana Sreedharan, Arun Kumar Kashyap, Pardeep Singh, and Nirala Ramchiary. "A Review on Bioactive Phytochemicals, Ethnomedicinal and Pharmacological Importance of Purslane (Portulaca Oleracea L.)." (2021).
7. Srivastava, Rajani, Vineet Srivastava, and Ajeet Singh. "Multipurpose Benefits of an Underexplored Species Purslane (Portulaca Oleracea L.): A Critical Review." *Environmental Management* (2021): 1-12.
8. Gallo, Monica, Esterina Conte, and Daniele Naviglio. "Analysis and Comparison of the Antioxidant Component of Portulaca Oleracea Leaves Obtained by Different Solid-Liquid Extraction Techniques." *Antioxidants* 6, no. 3 (2017): 64.
9. Khanam, Benazir, W Begu, and F Tipo. "Pharmacological Profile, Phytoconstituents, and Traditional Uses of Khurfa (Portulaca Oleracea L.): Unani Perspective." *Journal of Pharmaceutical Innovations* 8 (2019): 367-72.
10. Lingyu Li, Luping Yang, Yanni Jiao, Shuiyao Hu, Erlan Yang, Ping Li, Shubo Gu, and Lan Xiang. "Total Organic Acids from Ethanol Extract of Portulaca Oleracea Reduce Inflammation in Lps-Induced Sepsis Mouse Model." *Chinese Traditional Medicine Journal* 3, no. 2 (2020): 1-13.
11. Khodadadi, Hadi, Roghayeh Pakdel, Majid Khazaei, Said Niazmand, Kowsar Bavarsad, and Mousa AL-Reza Hadjzadeh. "A Comparison of the Effects of Portulaca Oleracea Seeds Hydro-Alcoholic Extract and Vitamin C on Biochemical, Hemodynamic and Functional Parameters in Cardiac Tissue of Rats with Subclinical Hyperthyroidism." *Avicenna journal of phytomedicine* 8, no. 2 (2018): 161.
12. Fu, Jia, Hongqing Wang, Chaoxuan Dong, Chuchu Xi, Jun Xie, Shengtian Lai, Ruoyun Chen, and Jie Kang. "Water-Soluble Alkaloids Isolated from Portulaca Oleracea L." *Bioorganic Chemistry* (2021): 105023.
13. Wang, Peipei, Hongxiang Sun, Dianyu Liu, Zezhao Jiao, Su Yue, Xiuquan He, Wen Xia, Jianbo Ji, and Lan Xiang. "Protective Effect of a Phenolic Extract Containing Indoline Amides from Portulaca Oleracea against Cognitive Impairment in Senescent Mice Induced by Large Dose of D-Galactose/Nano2." *Journal of ethnopharmacology* 203 (2017): 252-59.
14. Truong, Huynh Kim Thoa, Man Anh Huynh, My Dung Vuu, and Thi Phuong Thao Dang. "Evaluating the Potential of Portulaca Oleracea L. For Parkinson's Disease Treatment Using a Drosophila Model with Duch-Knockdown." *Parkinson's Disease* 2019 (2019).
15. Farag, Ola M, Reham M Abd-Elsalam, Hanan A Ogaly, Sara E Ali, Shymaa A El Badawy, Muhammed A Alsherbiny, Chun Guang Li, and Kawkab Ahmed. "Metabolomic Profiling and Neuroprotective Effects of Purslane Seeds Extract against Acrylamide Toxicity in Rat's Brain." *Neurochemical Research* 46, no. 4 (2021): 819-42.
16. El-Sayed, Mahmoud, Sameh Awad, and Amel Ibrahim. "Impact of Purslane (Portulaca Oleracea L.) Extract as Antioxidant and Antimicrobial Agent on Overall Quality and Shelf Life of Greek-Style Yoghurt." *Egyptian Journal of Food Science* 47, no. 1 (2019): 51-64.
17. Tleubayeva, Meruyert I, Ubaidilla M Datkhayev, Mereke Alimzhanova, Margarita Yu Ishmuratova, Nadezhda V Korotetskaya, Raisa M Abdullabekova, Elena V Flisyuk, and Nadezhda G Gemejiyeva. "Component Composition and Antimicrobial Activity of Co2 Extract of Portulaca Oleracea, Growing in the Territory of Kazakhstan." *The Scientific World Journal* 2021 (2021).
18. Darvish Damavandi, Reyhaneh, Farzad Shidfar, Mohammad Najafi, Leila Janani, Mohsen Masoodi, Maryam Akbari-Fakhrabadi, and Afsaneh Dehnad. "Effect of Portulaca Oleracea (Purslane) Extract on Liver Enzymes, Lipid Profile, and Glycemic Status in Nonalcoholic Fatty Liver Disease: A Randomized, Double-Blind Clinical Trial." *Phytotherapy Research* (2021).
19. Rahimi, Vafa Baradaran, Farideh Ajam, Hasan Rakhshandeh, and Vahid Reza Askari. "A Pharmacological Review on Portulaca Oleracea L.: Focusing on Anti-Inflammatory, Anti-Oxidant, Immuno-Modulatory and Antitumor Activities." *Journal of pharmacopuncture* 22, no. 1 (2019): 7.
20. Sharma, Alok, Gaurav Kaithwas, M Vijayakumar, MK Unnikrishnan, and Ch V Rao. "Antihyperglycemic and Antioxidant Potential of Polysaccharide Fraction from Portulaca Oleracea Seeds against Streptozotocin-Induced Diabetes in Rats." *Journal of Food Biochemistry* 36, no. 3 (2012): 378-82.
21. Yang, Xiaohang, Yongmei Yan, Jiankang Li, Zhishu Tang, Jing Sun, Huan Zhang, Siyang Hao, Aidong Wen, and Li Liu. "Protective Effects of Ethanol Extract from Portulaca Oleracea L on Dextran Sulphate Sodium-Induced Mice Ulcerative Colitis Involving Anti-Inflammatory and Antioxidant." *American journal of translational research* 8, no. 5 (2016): 2138-48.

22. Chandimali, Nisansala, Hyebin Koh, Jihwan Kim, Jaihyung Lee, Yang Ho Park, Hu-Nan Sun, and Taeho Kwon. "Brm270 Targets Cancer Stem Cells and Augments Chemo-Sensitivity in Cancer." *Oncology Letters* 20, no. 4 (2020): 1-1.
23. Jia, Guiyan, Xingyue Shao, Rui Zhao, Tao Zhang, Xiechen Zhou, Yang Yang, Tao Li, Zhao Chen, and Yupeng Liu. "Portulaca Oleracea L. Polysaccharides Enhance the Immune Efficacy of Dendritic Cell Vaccine for Breast Cancer." *Food Function* 12, no. 9 (2021): 4046-59.
24. Sdouga, Dorra, Ferdinando Branca, Souhir Kabtni, Maria Concetta Di Bella, Neila Trifi-Farah, and Sonia Marghali. "Morphological Traits and Phenolic Compounds in Tunisian Wild Populations and Cultivated Varieties of Portulaca Oleracea L." *Agronomy* 10, no. 7 (2020): 948.
25. Xing, Jie, Zijuan Yang, Beibei Lv, and Lan Xiang. "Rapid Screening for Cyclo-Dopa and Diketopiperazine Alkaloids in Crude Extracts of Portulaca Oleracea L. Using Liquid Chromatography/Tandem Mass Spectrometry." *Rapid Communications in Mass Spectrometry* 22, no. 9 (2008): 1415-22.
26. Jiao, Zezhao, Haina Wang, Peipei Wang, Hongxiang Sun, Su Yue, and Lan Xiang. "Detection and Quantification of Cyclo-Dopa Amides in Portulaca Oleracea L. By Hplc-Dad and Hplc-Esi-Ms/Ms." *J 中国药学*, no. 8 (2014): 3.
27. Jiao, Ze-Zhao, Su Yue, Hong-Xiang Sun, Tian-Yun Jin, Hai-Na Wang, Rong-Xiu Zhu, and Lan Xiang. "Indoline Amide Glucosides from Portulaca Oleracea: Isolation, Structure, and Dpph Radical Scavenging Activity." *Journal of Natural Products* 78, no. 11 (2015): 2588-97.
28. Voynikov, Yulian, Reneta Gevrenova, Vessela Balabanova, Irini Doytchinova, Paraskev Nedialkov, and Dimitrina Zheleva-Dimitrova. "Lc-Ms Analysis of Phenolic Compounds and Oleraceins in Aerial Parts of Portulaca Oleracea L." *Journal of Applied Botany Food Quality* 92 (2019): 298-312.
29. Xiang, Lan, Dongming Xing, Wei Wang, Rufeng Wang, Yi Ding, and Lijun Du. "Alkaloids from Portulaca Oleracea L." *Phytochemistry* 66, no. 21 (2005): 2595-601.
30. Liu, Dianyu, Tao Shen, and Lan Xiang. "Two Antioxidant Alkaloids from Portulaca Oleracea L." *Helvetica Chimica Acta* 94, no. 3 (2011): 497-501.
31. "Team, R Core. R: A Language and Environment for Statistical Computing. R Foundation for Statistical Computing, Vienna. Http S." www.R-project.org (
32. Kassambara, Alboukadel, and Fabian Mundt. "Package 'Factoextra'." *Extract, visualize the results of multivariate data analyses* 76 (2017).
33. Wickham, Hadley, Mara Averick, Jennifer Bryan, Winston Chang, Lucy D'Agostino McGowan, Romain François, Garrett Grolemund, Alex Hayes, Lionel Henry, and Jim Hester. "Welcome to the Tidyverse." *Journal of open source software* 4, no. 43 (2019): 1686.
34. Maechler, Martin, Peter Rousseeuw, Anja Struyf, Mia Hubert, Kurt Hornik, and Matthias Studer. "Package 'Cluster'." (2013).
35. Csardi, Gabor, and Tamas Nepusz. "The Igraph Software Package for Complex Network Research." *InterJournal, complex systems* 1695, no. 5 (2006): 1-9.
36. Galili, Tal. "Dendextend: An R Package for Visualizing, Adjusting and Comparing Trees of Hierarchical Clustering." *Bioinformatics* 31, no. 22 (2015): 3718-20.